FLORIDA INTERNATIONAL UNIVERSITY

Miami, Florida

GEOPHYSICAL ANALYSIS OF A CENTRAL FLORIDA KARST TERRAIN USING LIGHT DETECTION AND RANGING (LIDAR) AND GROUND PENETRATING RADAR (GPR) DERIVED SURFACES

A thesis submitted in partial fulfillment of the

requirements for the degree of

MASTER OF SCIENCE

in

GEOLOGY

by

Juana Maria Montané

2002

To: Dean Arthur W. Herriott
College of Arts and Sciences

This thesis, written by Juana Maria Montané, and entitled Geophysical Analysis of a Central Florida Karst Terrain using Light Detection and Ranging (LIDAR) and Ground Penetrating Radar (GPR) Derived Surfaces, having been approved in respect to style and intellectual content, is referred to you for judgment.

We have read this thesis and recommend that it be approved.

_____
Dr. Grenville Draper

_____
Dr. Michael Gross

_____
Dr. Dean Whitman, Major Professor

Date of Defense: July 27, 2001

The thesis of Juana Maria Montané is approved.

_____
Dean Arthur W. Herriott
College of Arts and Sciences

_____
Dean Douglas Wartzok
University Graduate School

Florida International University, 2002

ACKNOWLEDGMENTS

Many people helped and encouraged me in bringing this thesis to its present state, and I am so grateful to all of them. I want to thank and acknowledge Dr. Dean Whitman my advisor, as well as my committee members Dr. Michael Gross and Dr. Grenville Draper. Although the completion of this thesis was not the most conventional, they never failed to come through with advice and comments when needed.

I am eternally grateful to Dr. Whitman who taught me about practical, technical writing more than any class could. It is not easy to get people to read and critique a work in progress. Thanks from the bottom of my heart to my cherished friends the soon to be Dr. Martin Finn, Bobby Radakovich and George Anderson. Thanks to my little brother Robert, for his time and patience out in the field early in this study. Good luck in your endeavors at UF and congratulations.

When things threatened to drive me insane, four wonderful people came to my rescue. Thanks so much to Dean for always coming through at all stages of this study and for helping me to see the things that I could not. Thanks to Rosa Necolardes and Dr. William Anderson for your unwavering patience, advice and friendship on my bad days as well as the good through this endeavor. The same for Marty, who saw me through fieldwork (twice), computer glitches, personal glitches and who always seemed to bail me out of trouble more frequently than I would like to state.

Heartfelt appreciation to William Wilson P.G., and President of Subsurface Evaluations Inc. in Tampa, Florida for the use of his geophysical equipment, technical reports, time and being available anytime and every time I called upon him.

And finally, the best support in the world came from my mother, Gladys. She hasn't read one word of this thesis and possibly never will --but without her never faltering patience, love, understanding and encouragement this would not have come to fruition nor would I be where and who I am today. Thanks Mom, I love you dearly. Thanks to everyone mentioned and those not mentioned for countless moments of help towards this end.

ABSTRACT OF THE THESIS

GEOPHYSICAL ANALYSIS OF A CENTRAL FLORIDA KARST TERRAIN USING LIGHT DETECTION AND RANGING (LIDAR) AND GROUND PENETRATING RADAR (GPR) DERIVED SURFACES

by

Juana Maria Montané

Florida International University, 2002

Miami, Florida

Professor Dean Whitman, Major Professor

Airborne LIDAR (Light Detecting and Ranging) is a relatively new technique that rapidly and accurately measures micro-topographic features. This study compares topography derived from LIDAR with subsurface karst structures mapped in 3-dimensions with ground penetrating radar (GPR). Over 500 km of LIDAR data were collected in 1995 by the NASA ATM instrument. The LIDAR data was processed and analyzed to identify closed depressions. A GPR survey was then conducted at a 200 by 600 m site to determine if the target features are associated with buried karst structures. The GPR survey resolved two major depressions in the top of a clay rich layer at ~10m depth. These features are interpreted as buried dolines and are associated spatially with subtle (< 1m) trough-like depressions in the topography resolved from the LIDAR data. This suggests that airborne LIDAR may be a useful tool for indirectly detecting subsurface features associated with sinkhole hazard.

TABLE OF CONTENTS

CHAPTER PAGE

LIST OF FIGURES

FIGURE PAGE

Introduction

1.1 Background

Central Florida is a dynamic system of covered-karst terrain. Covered-karst terrains are simply defined as regions where soluble carbonate rocks are overlain by unconsolidated sediments (Beck and Sayed, 1991). The term 'Karst' has been adopted from its characteristic development in the karst region of Yugoslavia. In the United States, similar topography is found over large areas of Kentucky, Tennessee, Arizona, Indiana and Florida (Hinds, 1943). Karst terrains develop in response to dissolution of the limestone bedrock. In central Florida, karst is expressed in the rolling topography that lacks open drainage and consists of gently sloping depressions and sinkhole lakes formed by ancient karst processes.

Sinkholes (technically referred to as dolines) are ubiquitous features that primarily develop in the subsurface of karst environments. Closed, circular depressions are characteristic features of karst terrains and form due to subsidence of near surface sediments into cavities in the subsurface formed by dissolution. Often, sinkholes form rapidly due to active subsidence processes and have catastrophic results. Sinkholes constitute a significant geologic hazard in karst because of their inherent suddenness. Sinkholes are commonly funnel-shaped, measure a few meters to tens of meters and their general drainage is subterranean (Bates and Jackson, 1984). These features are the basic or index landforms of karst terrains (Ford and Williams, 1989).

For several decades, sinkhole development has increased and is particularly hazardous in populated areas (Newton, 1984). The effects of sinkholes in the past two

decades have raised public awareness and concern as well as helped change government policies. Such changes include regulating development and requiring geo-technical investigations of subsurface conditions and stability prior to development. The interaction between people and the environment results in extensive modification of natural processes. With the increasing population in central Florida such modifications include diversion of surface-water flow by housing and business developments, and highways that reduce the available ground in which natural waters may permeate. This causes changes in the surface and subsurface flow of waters that develop karst landforms and may induce or heighten high-risk areas. Modifications that affect the hydrologic head, such as over pumping which drops the surrounding water table, have been shown as a probable cause in the sinkhole collapse process (Sinclair, 1982; Beck, 1986; Chen and Beck, 1989; Beck and Sayed, 1991; Wilson and Beck, 1992; Upchurch and Randazzo, 1997; Whitman et al., 1999).

Sinkhole hazards range from modest subsidence with some structural damage to major catastrophic events resulting in subsurface re-stabilization, property loss and re-building. Formation of sinkholes damage roads, bridges, buildings, farmland, power lines and pipelines. Progressive subsidence and catastrophic events result in considerable financial loss to society and pose a major hazard to both humans and the environment. As more and more sinkhole collapse events have occurred, calls for predictive measures have become vigorous.

In light of increasing events, the NASA Topography and Surface Change Program (T&SCP) along with other federal, state and local agencies are engaged in research to better understand the evolution of karst landforms. These programs share a common goal

of developing a better interpretation for the formation and hydrologic framework of central Florida karst terrain, as well as other karst terrains in the country. Due to the increasing population in Florida, it is important to understand karst landform evolution and its effects on the land surface to better predict sinkhole hazard. Millions of dollars are lost in Florida each year to damage by sinkholes. Four million dollars alone was required for the damage resulting from the single collapse event in Winter Park, Florida in May of 1981 (Jammal, 1982; Upchurch and Randazzo, 1997).

Prediction of sinkhole collapse has been problematic or impossible considering that subsurface erosion is difficult to monitor and record. However, subtle surface topographic variations have been noted to reflect subsidence of the land surface by developing depressions (Sinclair et al., 1985; Wilson and Beck, 1988). It would be of great utility if topographic expressions could be used to detect possible future sinkholes, or areas at high risk for catastrophic sinkhole development.

Identified precursors to sinkhole collapse have been the slumping or slanting of fence posts or other objects, doors and windows that do not close properly, structural failure as in linear cracks in the walls, floors, pavement and the ground surface, and the ponding of rainfall (Wilson and Beck, 1988). Vegetative stress from a lowered water table and turbidity in well water are also indicative signs that occur during the early stages of a developing sinkhole (Sinclair, 1982). Ford and Williams (1989) have also indicated buried sinkholes as hidden geologic hazards where subsidence may re-occur.

A variety of geophysical techniques are used to investigate subsurface features related to sinkhole hazard. Conventional geophysical subsurface investigation methods, such as Ground Penetrating Radar (GPR), resistivity, induced polarization methods,

electromagnetic (EM) induction and borehole drilling are all time-consuming and expensive particularly in evaluating large areas. These more conventional approaches to the detection of cavities have not proven to be consistently effective nor do these methods work equally well (Sinclair et al., 1985). The amount of practical information derived from typical geo-technical techniques varies and they provide only limited temporal and spatial information. Regardless, these are commonly used as reliable methods. More precise techniques for prediction of sinkhole development have yet to be developed. However, sinkholes are ultimately connected to the surface therefore high-resolution detailed topography mapping may be useful as an alternative to mapping the subsurface. LIght Detection and Ranging (LIDAR) technology allows for detailed topographic measurements to be acquired precisely and easily over large areas.

To date, the highest resolution database available for the state of Florida are United States Geologic Survey (USGS) 1:24000 scale, 7.5 minute topographic maps with 5 or 10 ft (1.5 to 3 m) contour intervals. At this scale, only relatively large (>50 m) topographic features are resolvable. Furthermore, the hypsometry (methods used to describe accurately the elevations of the earth's surface) for these maps usually date back from the 1950's and 1960's making them grossly out of date. Most USGS topographic maps have been converted into raster format digital representations of the land surface commonly known as digital elevation models (DEMs). The horizontal resolution of these models is 30 meters and the root-mean-square-error (RMSE) of the vertical accuracy is 7 – 15 m (USGS, 1993). Exploring higher resolution and accuracy techniques to derive better DEMs is essential. The present available datasets are of an insufficient level of

detail and resolution for use in detecting pre-collapse sinkhole features at the centimeter level.

Airborne LIDAR technology, though relatively new can be used to accurately map the land surface topography. LIDAR works by transmitting laser light pulses from an airborne platform that once reflected back from surfaces below allows the distance to be calculated. Using the Global Positioning System (GPS), the LIDAR data is converted into measurements of land surface elevation relative to the Earth ellipsoid. LIDAR technology is time and cost-effective by rapidly and accurately measuring micro-topographic features, making this technology useful in efficiently producing surface maps for deducing subtle surficial features.

This study utilizes topographic data collected by NASA's Airborne Topographic Mapper (ATM) that is able to measure large regions of micro-topography with resolutions of 15-20 cm in a few hours (Krabill et al., 1995b). In a selected study site, ground-penetrating radar (GPR) is used to map the subsurface reflections associated with the ATM derived topography. The maps are then compared in a Geographic Information System (GIS) in order to better understand surface topography related to subsurface structures.

1.2 General Geologic Setting

Florida, along with Georgia and South Carolina are a part of the Southeastern Coastal Plain. Predominantly carbonate sediments with periodic deposition of siliciclastic sediments make up the Florida Platform. Florida's physiographic features and general low relief are a result of a limestone platform that has been locally uplifted and differentially dissolved. Throughout the Mesozoic and Cenozoic eras, shallow

marine sediments have accumulated in an off-lapping succession on the Atlantic coast and on the west coast during the development of the Gulf of Mexico basin (Beck, 1986). The Florida platform has seen repeated sea level changes that have caused erosion and deposition that reworked the sediments of the uplands (White, 1970; Beck, 1986; Randazzo, 1997; Schmidt, 1997; Scott, 1997).

Central Florida is composed of mainly Cenozoic carbonate and clastic strata. There is Eocene to Holocene age strata exposed at the surface (Figure 1.1). During the Eocene and Oligocene, a high stand of sea level allowed for major production of carbonates that covered most of the platform. The carbonates deposited at this time make up the Lake City Limestone that is known to have formed 43.6 – 52.0 million years ago with the total thickness unknown (Table 1.1). Overlying the Lake City limestone is the Avon Park Limestone that is 120 - 180 m thick and formed 40.0 – 43.6 million years ago. Above this is the Ocala Group, which formed 36.6 – 40.0 million years ago and is less than 60 m thick (Sinclair and Stewart, 1985; Florida Geological Survey, 1986; Wilson and Beck, 1992). These layers are composed of soft to medium, cream and tan sands and at greater depths the composition is a harder dark brown crystalline dolomite sedimentary rock with chalky fossiliferous layers of limestone. The Oligocene and Eocene strata are exposed on the west central part of the Florida peninsula (Figure 1.1). During the late Oligocene, there was a low stand of sea level, which saw the end of the Georgia Channel that had regularly prohibited siliciclastic sediments from being deposited southward.

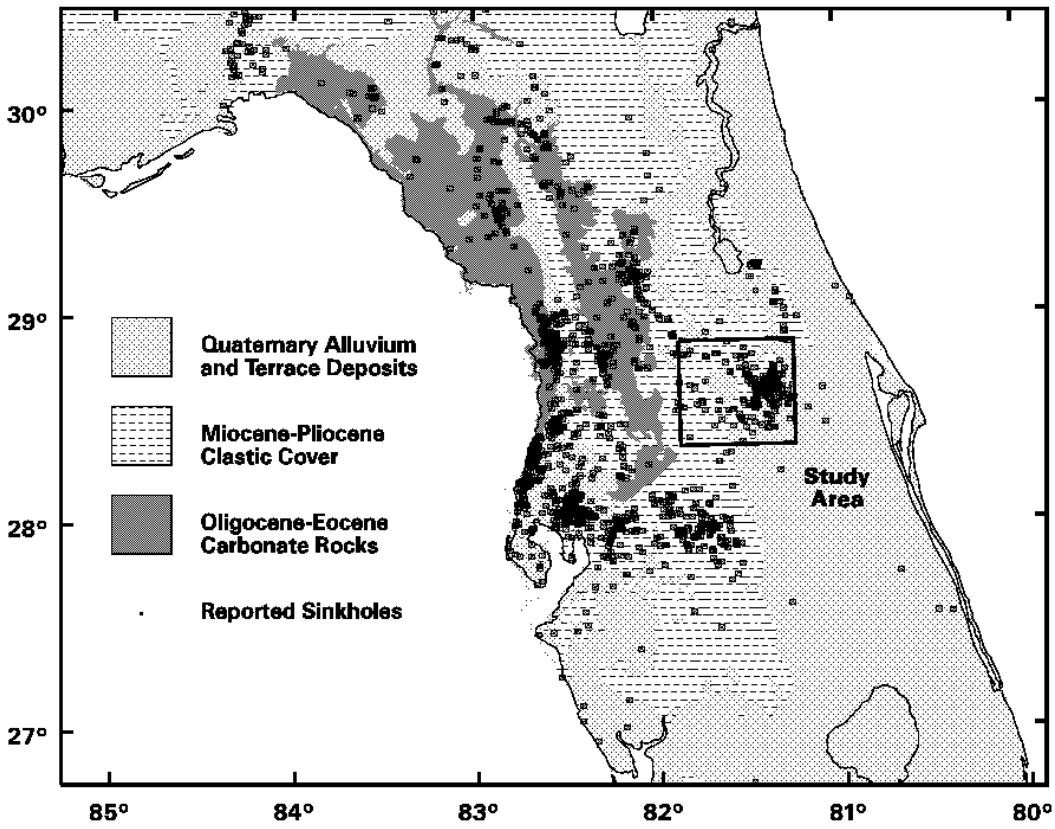

Figure 1.1 Simplified geologic map of the Florida Peninsula (courtesy of the Florida Geological Survey). Holocene through Miocene units are exposed along the eastern side of the state and Eocene through Miocene units are exposed along the western side. The study area is enclosed in the box and the points indicate the locations of reported sinkholes that occurred between 1960 and 1993 compiled by the Florida Sinkhole Research Institute (Spencer and Lane, 1995).

Table 1.1 Generalized Geologic and Hydrogeologic Units of Central Florida Modified from Sinclair and Stewart, 1985; Florida Geological Survey, 1986; Wilson and Beck, 1992).

System	Series	Thickness (m)	Strat Unit	Lithology	Hydrogeology Unit
Quaternary	Pleistocene to Recent	0 – 20	Undifferentiated deposits	Fine to med sand w/shell and clay	Surficial Aquifer
Tertiary	Pliocene	20 – 40	Caloosahatchee Formation	Undifferentiated limestone w/shell and clay layers	Confining Bed
	Miocene	40 – 100	Hawthorn Group	Phosphatic Limestone w/dolomite, silty sand and clay	Intermediate Aquifer
	Oligocene	100 – 110	Suwannee Formation	Fossiliferous, sandy limestone	Confining Bed
	Eocene	110 – 170	Ocala Group	Chalky limestone w/ fossils and dolomite	Floridan Aquifer System (Upper Floridan)
		170 – 320	Avon Park Limestone	Limestone w/crystalline dolomite	Middle Confining Unit
		320 – ?	Lake City Limestone	Limestone w/ crystalline dolomite layers and quartz	(Lower Floridan)

Siliciclastics began to be intermittently deposited throughout the Miocene forming the Hawthorn Group that consists of limestone with dolomite, phosphatic sand, silty-sand and clay (Sinclair et al., 1985; Wilson and Beck, 1992). The siliciclastics are eroded from the southeastern coastal plain and southern Appalachians. By the middle Miocene, the clay to clayey-sands completely covered Eocene and older carbonates on the Ocala Platform (Scott, 1997). The large and frequent sea-level fluctuations reworked the older sediments with younger sediments, especially in the latter portion of the Miocene. During the late Miocene the siliciclastic sediments prograded into the shallow, carbonate producing waters covering the limestone and forming the spine of the clayey sands on the Florida peninsula (Schmidt, 1997). Following the dramatic lowering of sea level in the Miocene, the sea level rose during the Pliocene as shown in the distribution of sediments (Scott, 1997). Mainly, the Pliocene sediments were deposited in a marine environment but a strong influence of siliciclastics from the north continued. The latter Pliocene low sea level conditions resulted in an increased rate of siliciclastic sediment dispersal onto the Florida platform and suppressed carbonate production. Erosion, dissolution and coastal processes re-working the sediments with non-marine and deltaic medium to fine grain sands produced much of the landscape seen today.

Throughout the Pleistocene, the sea did not rise to cover all of the Florida Platform. For the most part, much of central and northern Florida remained subaerially exposed, karstification and erosional sequence-boundary surfaces developed. In this region of central Florida, shallow closed depressions have commonly been associated with the predominantly siliciclastic Plio-Pleistocene sediments (Sinclair and Stewart,

1985; Miller, 1997; Randazzo, 1997; Upchurch and Randazzo, 1997). Throughout the Holocene, the sea level rose to its present level leaving the Florida Platform partially exposed, as we observe it today (White, 1970; Randazzo, 1997; Schmidt, 1997; Scott, 1997). The younger strata are exposed in the north, central and eastern portions of the state (Figure 1.1).

Florida is underlain by an extensive system of aquifers. Three distinct hydrostratigraphic units exist in north and central Florida: The Floridan aquifer, the intermediate confining unit, and the surficial aquifer system (Florida Geological Survey, 1986; Miller, 1997). The Floridan aquifer extends throughout the state of Florida, underneath large areas of Georgia and smaller areas of South Carolina and Alabama (Miller, 1986). The lower portion of the Floridan is composed of the Lake City Limestone, the Avon Park Limestone, the Ocala group and the Suwannee group. The Suwannee group however, is completely eroded in some areas including the study site (Table 1.1). Limestone with alternating layers of dolomite, some quartz and chalky fossiliferous limestone make up the lower portion of the Floridan. The Floridan aquifer has been subjected to extensive dissolution and cavity formation and supplies most of central and north Florida with their potable water (Wilson and Beck, 1992; Miller, 1997). Where it is confined, it is capped by an aquitard of variable thickness known as the intermediate confining unit. The sediments are of Miocene age, clay rich clastic sediments that makeup the Hawthorn group. Above the Hawthorn are thin Pliocene to Pleistocene permeable undifferentiated sediments of fine to medium sand with occasional shell and clay layers that form the surficial aquifer system (Sinclair and Stewart, 1985; Florida Geological Survey, 1986; Wilson and Beck, 1992; Miller, 1997). The surficial

aquifer system is unconfined and discontinuous throughout the region. The interplay between the surficial and Floridan aquifers is essential in understanding the sinkhole phenomena in central Florida. Whitman et al. (1999) have shown that a large positive head difference between the surficial and Floridan aquifer systems can be a major driving force in sinkhole collapse.

Central and north Florida's landscape is densely dotted with large lakes and ponds that are paleo karst depressions filled with water, a result of dissolution of the limestone bedrock. The topography is mainly rolling hills with sinkhole lakes and basins. Three distinct physiographic features border the region consisting of the Lake Wales, Mt. Dora and Orlando sand covered ridges (Figure 1.2). These paleo beach ridges are composed of thick unconsolidated sediments of fine to coarse quartz sands with occasional shell and clay layers (White, 1970; Scott and Hajishafie, 1980; Wilson and Beck, 1992). The ridges range in elevation from 27 to 94 m and are perforated by karst features.

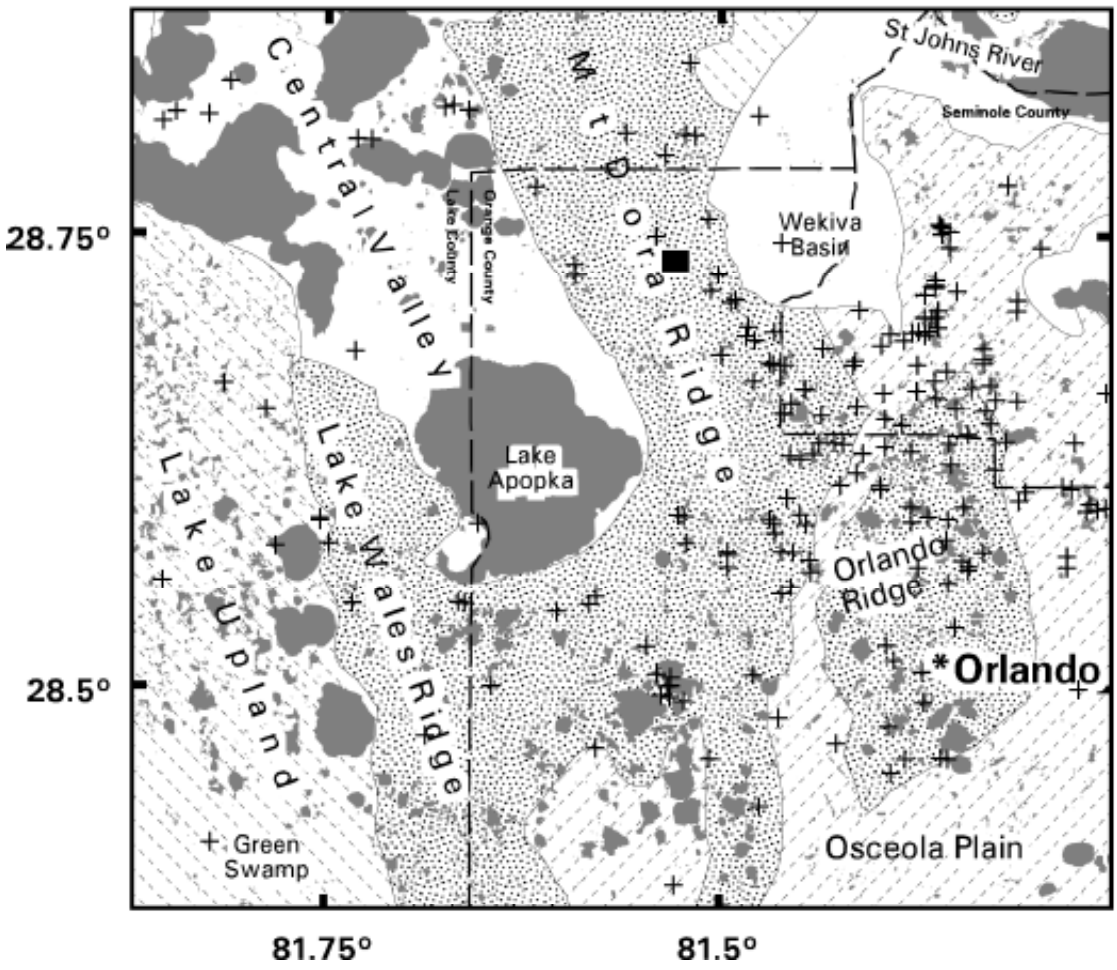

Figure 1.2 Generalized physiographic map of the study area with the study site in the black box. Areas of high topography are indicated in the stippled pattern, intermediate topography in the dashed pattern, and the lowest topography is in white. Crosses indicate sinkhole occurrences documented in the Florida Sinkhole Research Institute database (Spencer and Lane, 1995). Physiographic provinces are modified after White (1970).

1.3 Sinkholes in central Florida

Sinkholes in Florida are unpredictable features that form discreetly in the subsurface from dissolution and erosion. When sinkholes form rapidly, there are often catastrophic results (Culshaw and Waltham, 1987). Sinkhole development begins with

void space created by the dissolution of the limestone beneath. The process continues as sand from the overlying cover moves downward to fill solution cavities in the carbonate units (Beck 1986, Ford and Williams, 1989). During the formation, clayey cohesive sediments may bridge the cavity as it grows upward. Collapse occurs when the cohesive strength of the bridge is overcome by the weight of the overburden and the clayey sands are washed downward into the carbonate cavities. Wilson and Beck (1988) describe regions of covered-karst as areas where unconsolidated sands and clays have subsided or collapsed into solution cavities, with various reflecting topographic expressions at the land surface. However, surface expressions may not be apparent where the overlying sediments have filled and buried the karst features. Sinclair and Stewart (1985) identify major types of sinkholes common to west and central Florida these are: limestone solution, cover-subsidence and cover-collapse.

Limestone solution sinkholes predominate in areas where the limestone is bare or thinly covered by overlying material. The overlying materials subside at approximately the same rate as dissolution of the limestone and form shallow, broad depressions. Cover-subsidence sinkholes occur where the cover is relatively thick, non-cohesive, permeable sand. This occurs gradually as cover material moves downward into solution cavities in the limestone and develops funnel shape features. Cover-collapse sinkholes form where the overlying sediment is a clay-rich layer with sufficient cohesiveness to bridge developing cavities in the limestone until eventual and abrupt failure results in steep-sided depressions (Figure 1.3). Cover-collapse sinkholes pose the greatest hazard and have been identified as the main type of sinkhole that develops in central Florida

(Jammal, 1982; Sinclair et al., 1985; Wilson and Beck, 1992). Ultimately, the size of the depression is dependent on the amount of overburden material the cavity can accept.

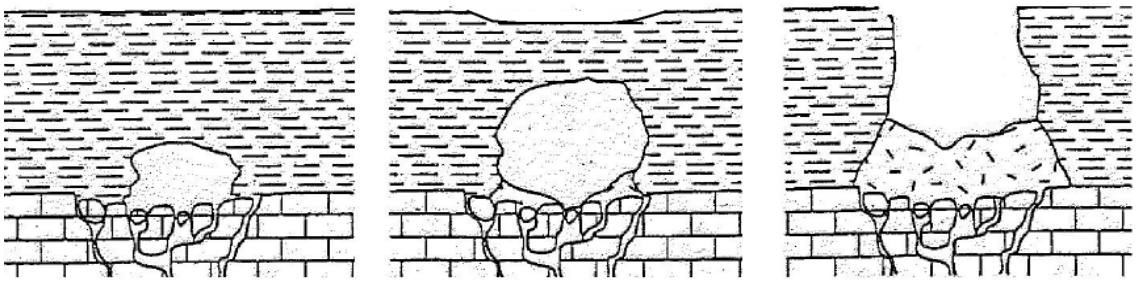

Figure 1.3 A simplified model of a developing cover-collapse sinkhole. **A.** The process is initiated by dissolution of the limestone beneath. **B.** As the cavity grows upward, the cohesive sediments bridge it. **C.** Collapse occurs when the cohesive strength of the bridge is exceeded by the weight of the overlying material. (Modified after Sinclair et al., 1985).

In areas underlain by limestone and other soluble rocks, sinkholes are a natural and common geologic hazard. All types of sinkholes become exceedingly dangerous and disastrous when occurring in highly populated areas. An example of a catastrophic sinkhole collapse occurred in Winter Park, Florida in May of 1981. This sinkhole is believed to be either a cover-collapse type or a re-activated paleo-sinkhole buried deep in the karst terrain (Upchurch and Randazzo, 1997). Buried sinkholes constitute a hidden geologic hazard where subsidence has and may re-occur (Culshaw and Waltham, 1987). Sinkholes cause damage to buildings, infrastructure, farmland and the environment. An additional environmental hazard is the drainage of ponds and lakes that allow direct infiltration of contaminated surface waters into the aquifer (Wilson and Beck, 1988).

1.4 Objectives

Sinkhole collapse events may be preceded by topographic indicators (Figure 1.3 B), which are too subtle to be represented on conventional topographic maps. In order to test the hypothesis that LIDAR derived topography can detect subtle topographic features associated with subsurface structures, the LIDAR data must be compared with subsurface features mapped with conventional methods such as GPR. If topographic precursors to sinkhole collapse exist, are they features that are smaller than what can be found on topographic maps? Is it possible to predict future sinkholes by these topographic indicators? If so, then airborne LIDAR technology may be used to map subtle topographic features which can then be used to delineate precursors for sinkhole hazard mitigation.

Beyond this possible application for sinkhole hazard, a detailed comparison of the LIDAR derived micro-topography with corresponding structures or interfaces will lead to a better understanding of karst terrain and karst geomorphology. Karst topography forms in response to subsurface erosion ultimately linking sinkholes to the surface. The main objective of this study is to compare the topography derived from LIDAR technology collected by NASA's airborne topographic mapper (ATM) and subsurface features mapped with ground penetrating radar (GPR). From the comparison, it is necessary to determine if the targeted surface features are associated with buried karst structures. Exploring the relationship between subtle features in the surface topography and subsurface erosion will advance the understanding of how topography evolves in karst terrains. Thus, improving our understanding of karst landform evolution.

In chapter 2, airborne LIDAR technology is discussed inclusive of how the dataset for this study was acquired and processed. This chapter also discusses the visualization procedure, intent and exactly how targets and a smaller study site was chosen for a more detailed investigation. From this a ground truth land survey was completed to quantify the error of the ATM data set within the study site. This is explained in section 2.5.1. In section 2.5.2 a comparison of the ATM topography and a USGS topographic map is presented and quantitatively reveals the relevance of employing LIDAR derived digital elevation models (DEMs) versus conventional USGS DEMs. Chapter 3 provides a summarized background and explanation of ground penetrating radar (GPR) techniques. The GPR data collected, how the data was utilized in this analysis and interpreted to explore the relationship between surface and subsurface features is presented. Chapter 4 offers a discussion of the observations made and a direct comparison of the LIDAR and GPR derived surfaces. Included in chapter 5 is a summary of this study and how it relates to the stated hypothesis.

In this study, micro-topography of a central Florida site is compared to corresponding subsurface structures and a relationship is investigated using spatial analysis techniques within a Geographic Information System (GIS). GIS is a useful tool that offers the ability to organize, visualize, merge and quantitatively analyze spatial datasets from various sources. Successful management and mitigation of sinkhole hazard in karst regions depends on understanding the development of this natural phenomenon at the subsurface and the surface.

2. Topography

2.1 LIDAR Data

LIDAR (light detection and ranging) technology has been used routinely on the ground to measure distances along survey lines in conventional surveying methods (Ritchie, 1995). Applying this technique from an airborne platform advances topographic mapping by accurately measuring large areas quickly and easily. LIDAR works by sending out short laser light pulses (nanosecond or less). Once the laser is shot, the electronics start timing. Timing stops once the echo returns and the receiver measures the lapse in time between the pulse initiation and its return (Ritchie, 1996). The distance to the ground, or other objects such as trees, buildings or power lines, is then calculated by the two-way travel time (twtt) multiplied by the velocity of light and divided by two. Active sensing systems, as opposed to passive instruments such as cameras, offer advantages in the acquisition and quality of data in areas of low relief.

A combination of three individual main components is used: laser range finders (LIDAR), highly accurate inertial navigation systems (INS) and the global positioning satellite system (GPS). An aircraft instrumented with these components provides the following: laser range to the Earth's surface, a measurement platform for spatial location and orientation, and aircraft kinematic trajectory in ellipsoidal coordinates (Vaughn et al., 1996). A schematic of the integrated subsystems mounted on an aircraft is shown in Figure 2.1. The differential GPS allows for the flight path and altitude of the aircraft to be measured accurately. The position of the laser platform must be known accurately to determine the flight path over the land surface (Krabill and Martin, 1987). During post-

processing the INS orientation and GPS position solutions are combined with the laser ranges to calculate accurate XYZ coordinates for each laser return. This combination of data is sufficient to produce accurate digital topographic maps of the terrain beneath the flight path of the aircraft. This emerging survey technology is capable of rapidly generating high-density, geo-referenced digital elevation data with accuracy similar to or better than traditional land surveys.

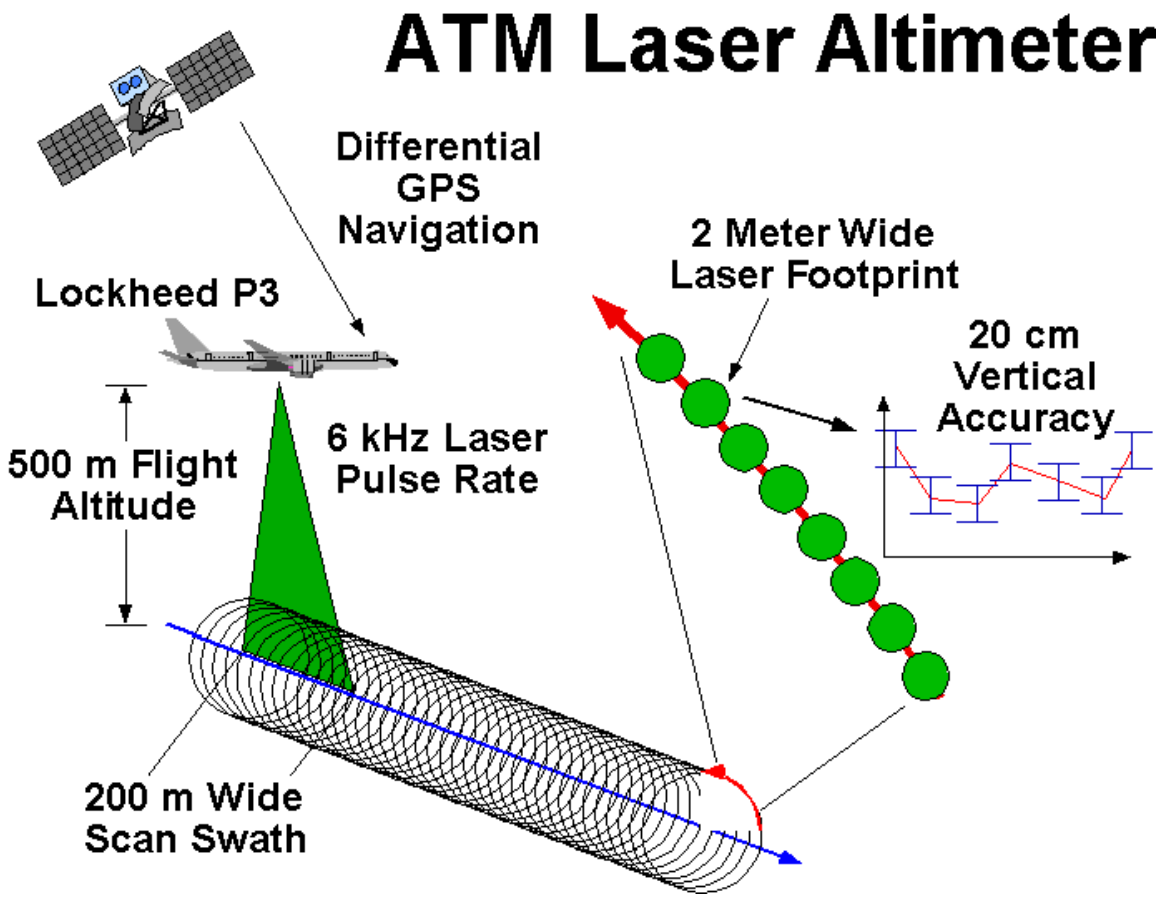

Figure 2.1 Schematic diagram showing the components of the ATM system with the acquisition parameters used for this study.

Applications of scanning laser altimeter systems provide raster or conical scans of the surface that can be used to make three-dimensional measurements of the landscape

surface (Krabill and Collins, 1984). The versatility of airborne laser data is shown in successful studies for mapping sea ice thickness and topography (Krabill et al., 1995a), vegetation properties and land surface topography (Ritchie, 1995; Ritchie et al., 1996) as well as in bathymetry studies (Guenther et al., 2000). ATM data has also been used in hydrologic studies (Ritchie, 1996), beach mapping (Krabill et al., 2000; Whitman, 2000) and hurricane storm surge hazard studies (Whitman et al., 2001).

The NASA airborne topographic mapper (ATM) was one of the first practical LIDAR systems to be used for collecting topographic data. It uses a single pulse laser sensor that produces a 200 m wide helical scan swath pattern with a pulse footprint spacing of 2 m (Figure 2.1). The ATM laser altimeter measures 6000 returns per second. Such measurements allow the determination of the landscape utilizing a rotating scan mirror that generates a high-density helical footprint along the flight path. The accuracy of the elevation data derived from the ATM system is known to be 10 – 20 cm (Krabill and Martin, 1987; Krabill et al., 1995b).

2.2 Data Acquisition

In November 1995, a NASA P-3 aircraft, equipped with the ATM instrument was deployed at an elevation of 500 m over the study area in an oval flight pattern about Lake Apopka in central Florida. The deployed 6000 kHz LIDAR scanner system generated over 17 million irregularly spaced laser returns within a helical scan pattern. The study recorded more than 500 km of overlapping swaths. Coincident lines from the helical scan pattern were merged into two north to south trending swaths, one 800 m wide over the Mount Dora ridge to the east of the study area and the second 600 m wide over the Lake Wales ridge to the west of the study area (Figure 2.2). Two other 200 m swaths

trending southwest to northeast were collected, one is to the southwest and the other is to the southeast of Lake Apopka. The total area covered by overlapping swaths in this study is 150 km^2. The helical pulsed LIDAR scanner returned values of height and intensity for each data point. The high-sampling rates attained make it possible to collect and rapidly complete an extensive *in situ* high-density topographic survey of the area.

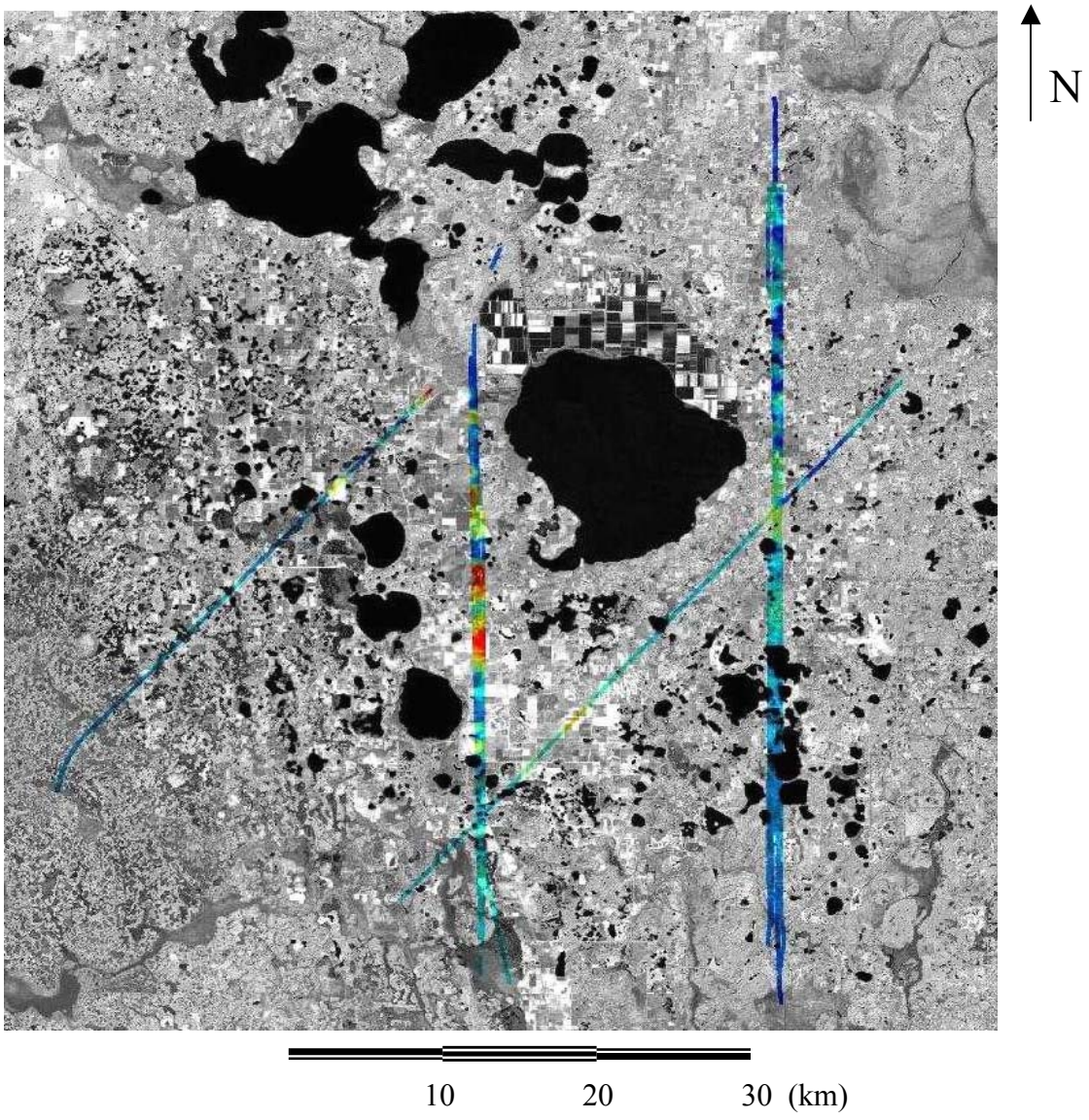

Figure 2.2 Satellite image of central Florida with ATM dataset superimposed. Elevations are color-coded: the highest elevations are in red and the lower elevations in blue. The black rectangle in the northeast corner is the location of Figure 2.3.

2.3 Processing

The data from each individual swath was delivered from NASA in a binary XYZ format. Each flight swath contained multiple fields including the latitude, longitude, ellipsoidal height and the reflection intensity for each laser pulse. The helical geometry of the scan pattern made interpretation of the raw data exceedingly difficult without extensive post-processing. Data from adjacent scans were merged and subdivided into 0.01 degree latitude (~1 km) tiles for each swath. Each tile contained between 100,000 and 250,000 points. Geodetic coordinates (latitude and longitude) were projected into a planemetric coordinate system (UTM, zone 17, NAD 83 datum). Ellipsoidal heights were converted to NAVD88 orthometric heights with the NGS Geoid96 model.

Irregularly spaced elevations are difficult to visualize in most GIS software. In order to visualize the data, elevations from the irregularly spaced points were interpolated onto a 2.5 m resolution grid using Dellaney triangulation. A grid of regularly spaced elevations is commonly called a digital elevation model (DEM). The 2.5 m cell size was chosen in order to be consistent with the 2 m point spacing of the helical scans. A 10 m search radius was used to prevent gridding in poorly controlled areas.

The unfiltered, gridded data resolved most of the features (Figure2.3A). However, due to vegetation, interpretation was difficult. In order to remove the vegetation, a terrain filter was run on the initial set of irregularly spaced points. Each grid cell contains both ground and non-ground surface reflections. Therefore, it is best to perform such filtering on the raw, irregularly spaced data points rather than the gridded dataset (Whitman et al., 2001). The filtered points were then re-gridded to produce a "bare ground" 2.5 m DEM. Next, a 3 x 3 focal mean filter was run on the DEM to

smooth out the remaining helical artifacts (Figure 2.3B). The laser scanner data is comprised of hundreds of thousands of points and removal of the vegetation and helical artifacts is difficult without losing ground data points. Color shaded relief maps of the LIDAR topography were produced in ERMapper and used to define and determine closed circular features.

2.4 Visualization and Identification of the Study Site

The occurrence of sinkholes (Figure 1.1) and the physiography (Figure 1.2) in the Orlando area were the reasons this region was selected for the study. The study area for this project is an 83 x 84 km region in central Florida (Figure 2.2). This region is comprised of parts of Orange, Osceola, Lake, Seminole, Marion, Polk, Putnam, and Volusa counties. It lies within the management boundaries of the South Florida Water Management District (SFWMD), St. Johns River Water Management District (SJRWMD), and South West Florida Water Management District (SWFWMD).

Within the study area, there were promising 'target' depressions (Figure 2.3A). A smaller site was chosen for a more detailed investigation (Figure 2.3B). This study site covers an area approximately 200 x 600 m located 30 miles west of Orlando in Apopka, Florida (Figure 2.4). The topography of this area typically consists of small rolling hills within larger prairies bounded by agricultural residences to the north and east. In this area of higher elevation than the majority of the state of Florida, oak and pine vegetation is abundant. The land to the west and south are owned by the city of Apopka, and is adjacent to the Northwest Water Treatment facility managed by the city of Apopka, SJRWMD and Orange County.

The objective of this exercise was to find closed circular depression not found on USGS topographic maps. Filtering techniques, linear stretches and sunshading filters were used to interactively explore the LIDAR dataset. Through this visualization, several depression features (targets) were identified. The targets were chosen for their closed, circular morphology and elevation. Seventy potential targets were identified and selected for field reconnaissance to confirm their existence and accessibility for the GPR survey. In the summer of 1999, several field excursions successfully verified 16 of these targets as real, closed depression type features. From the 16, only seven were accessible enough for a subsurface survey. Four of these were located in an area owned by the city of Apopka. A detailed investigation was completed at this selected study site (Figure 2.3B).

For the large amount of LIDAR coverage, the results were somewhat disappointing. The targets detected were semi-circular to oval in shape and were not completely closed features or at the scale expected. This was due in part to the noise (instrument and vegetation) in the LIDAR data that limited resolution. Another reason perhaps, for the lack of small-scale circular features is the geology in the area. The clastic cover here is of moderate thickness (>20 m - <100 m) and consists mainly of cohesive clayey sediments with low permeability (Sinclair et al., 1985). This type of sediment cover may inhibit the small-scale features from developing at all.

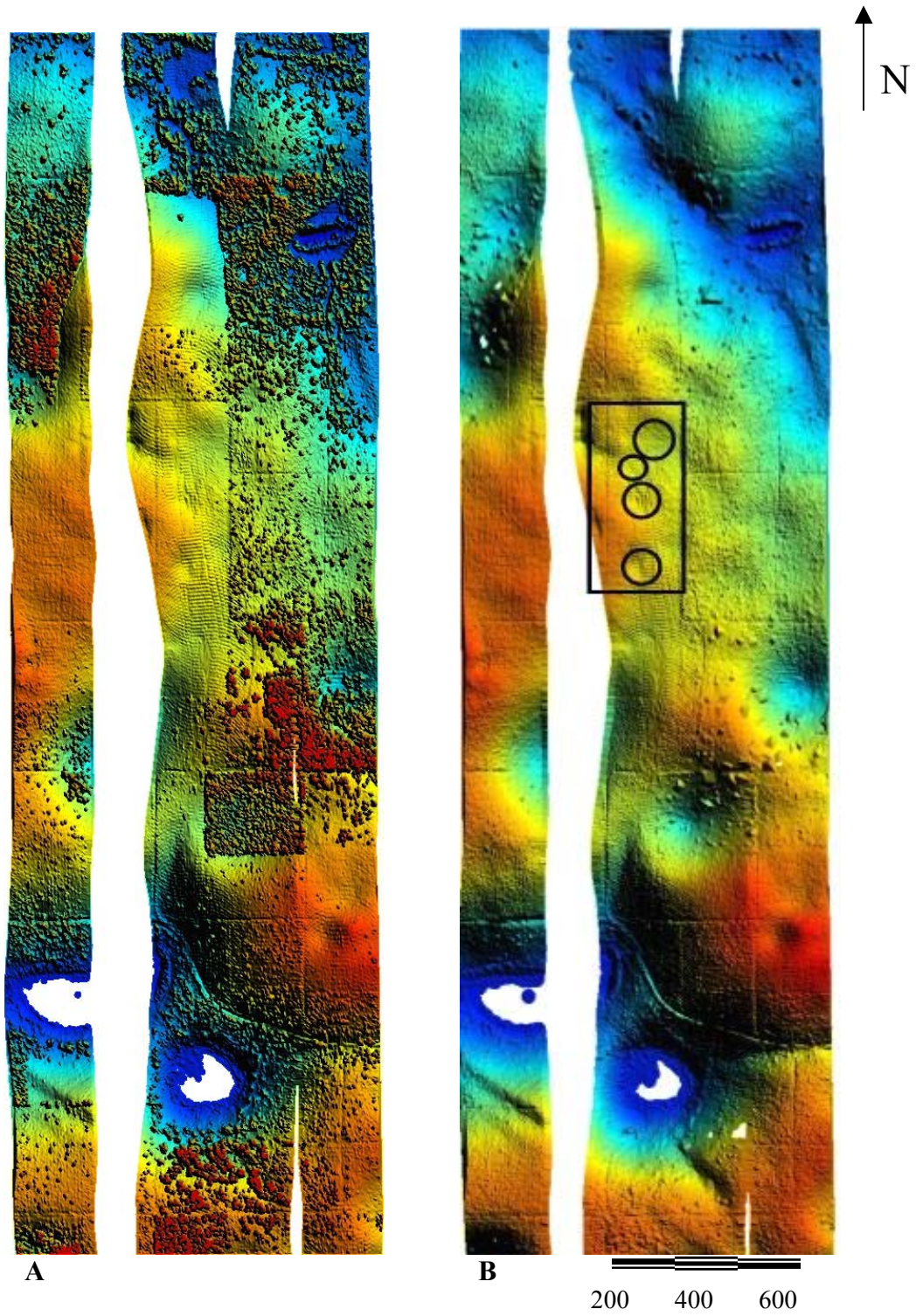

Figure 2.3 Shaded relief images of ground topography depicting filtering technique with targets circled. **A** is unfiltered; **B** is filtered with the location of the targets and study site (Figure 2.4) in the box. The helical artifacts are visible. Sunshading is at 45 degrees from the NNE. Elevation is color-coded with high areas in red and low areas in blue. White indicates areas of no data.

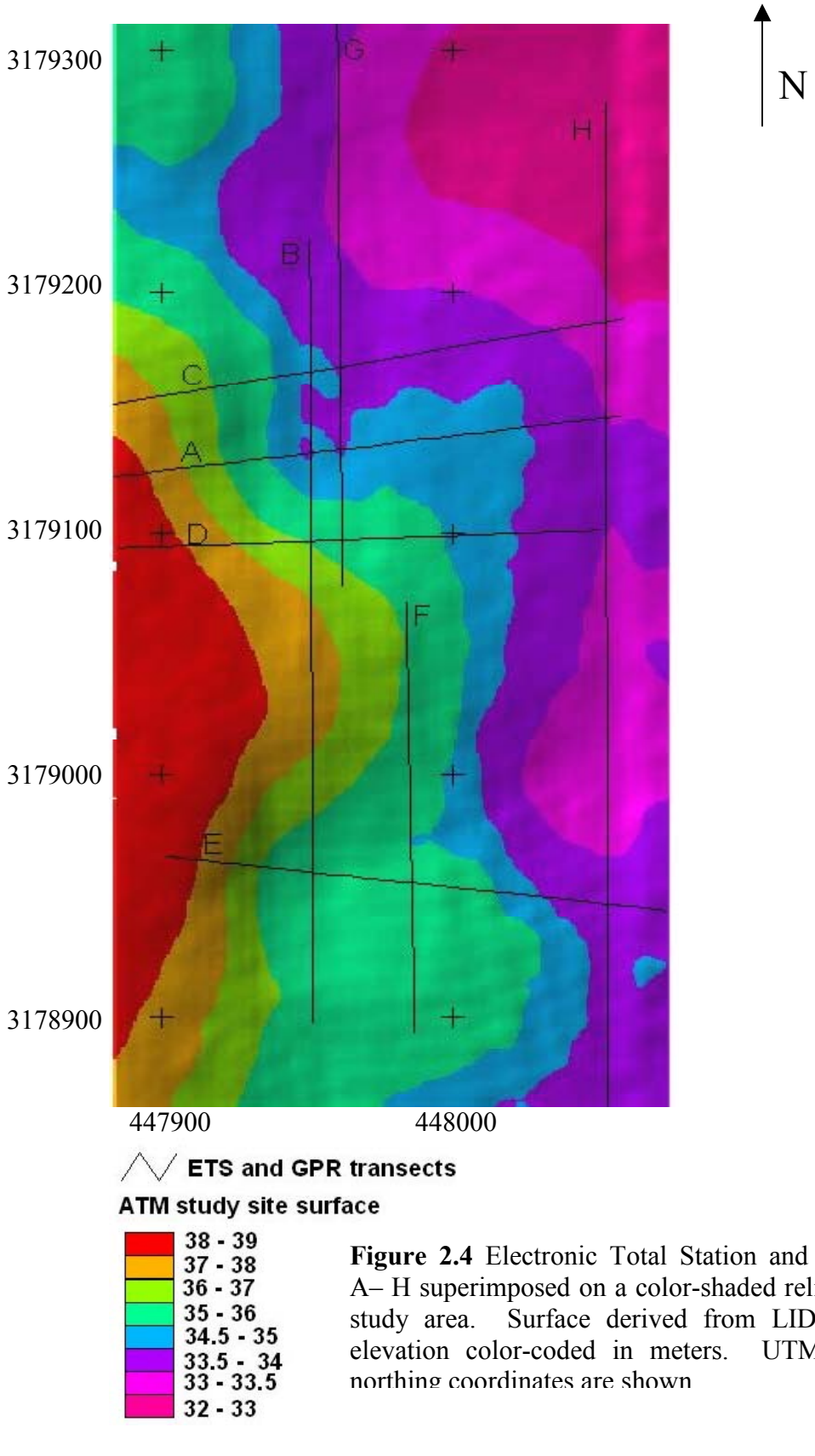

Figure 2.4 Electronic Total Station and GPR transect A– H superimposed on a color-shaded relief map of the study area. Surface derived from LIDAR data and elevation color-coded in meters. UTM easting and northing coordinates are shown

2.5 Comparisons

2.5.1 Airborne Topographic Mapper vs. Electronic Total Station

An electronic total station (ETS) was used to survey the site for a ground truth or quality check. Its purpose was to test and quantify the accuracy of the LIDAR data. The placement of the survey lines was determined by intersecting the targets detected at the study site to attain a cross-section of the features (Figure 2.4). The data was collected with the Leica electronic total station (ETS) TCR 305 and control points were established from benchmark 0490.

The reference point is located approximately two miles from the site. Dual GPS Magellan Pro Mark X receivers were used to collect coordinate data of the flagged reference points at the site. The data was then differentially post-processed and referenced back to a monitoring well at the water treatment plant adjacent to the study site. The reference points and azimuth information was input into the total station to accurately locate and orient the ETS. For detailed mapping over short distances the total station is capable of measuring between 3 – 5 mm accuracy over a km in a few seconds (Philpotts et al., 1997). A total of 123 points were collected across four targets.

The eight surveyed transects were labeled A through H and were also used as guides in the GPR survey. The points recorded were used to construct topographic cross-sections for direct comparison with the LIDAR data. From the unfiltered LIDAR DEM, coincident profiles were extracted using the geographic control points for each transect. The results of the elevation differences are necessary to obtain any systematic errors or offsets in the data caused by instrument malfunction or processing blunders (Whitman et al., 2001).

The root mean square was used to provide a quantitative estimate of the error. The National Standard for Spatial Data Accuracy (NSSDA) defines the RMSE to be the square root of the average of the squared differences between dataset coordinate values and coordinate values from an independent source of higher accuracy (FGDC, 1998). The resulting measure of absolute error is 18.9 cm with a mean offset of 17 cm. The reported level of accuracy for the ATM is approximately 20 cm (Krabill and Martin, 1987; Krabill et al., 1995b). Our values compared well and within the recognized error of the instrument (Figure 2.5). The mean difference most likely results from GPS and INS errors. The standard deviation was 7.9 cm. This is a measurement of relative error along transects and is equivalent to the RMSE if the mean offset is removed from the data. This tells us the minimum vertical resolving power of the LIDAR data and is useful for determining the depth of features that are likely to be detected. Overall, the results of the ETS survey positively assured the accuracy of the LIDAR data.

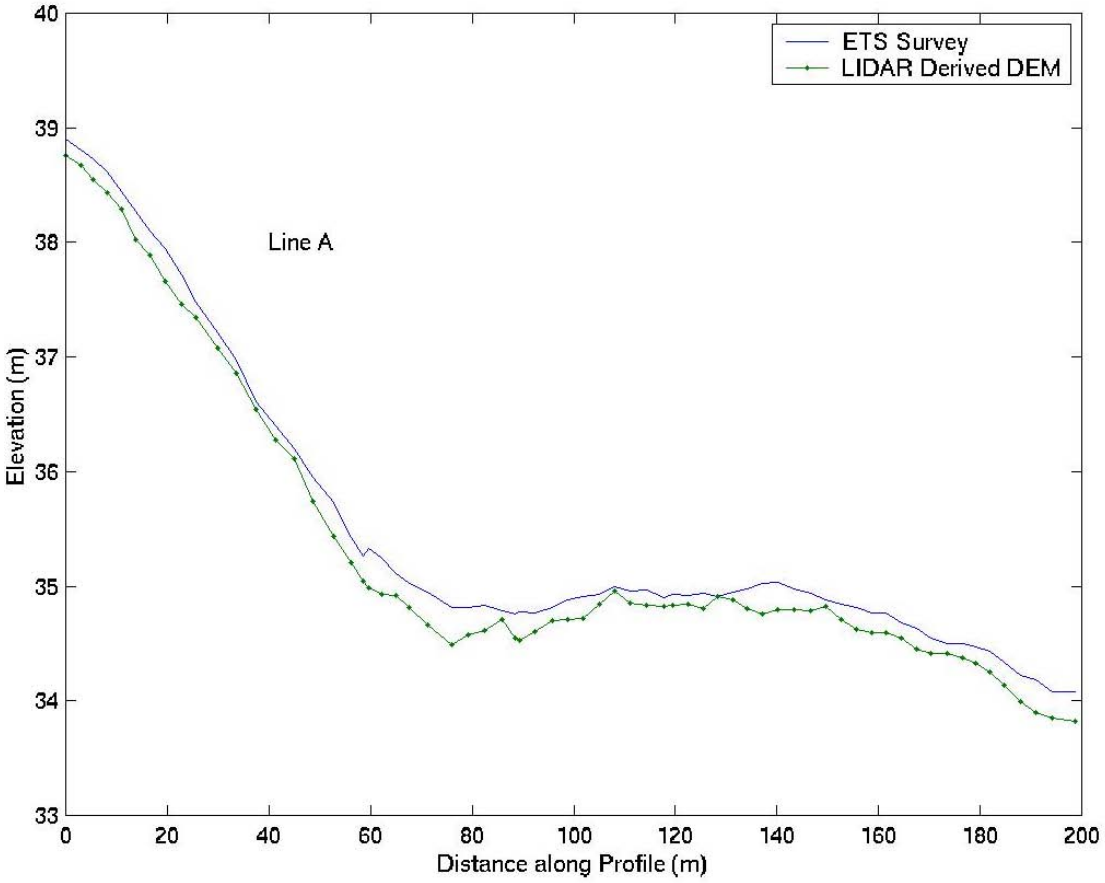

Figure 2.5 Example of comparison between electronic total station and ATM data. The ETS profile is in blue and the LIDAR profile in green. There is approximately 20 cm difference throughout all eight profiles, which is within the instrument error.

2.5.2 ATM data vs. USGS topographic map

A comparison with a United States Geologic Survey (USGS) topographic map and DEM derived from the ATM data was performed. This comparison shows the resolving power between the two datasets and describes the inaccuracies of the USGS topographic map. As previously stated in section 1.1, the best existing topographic resolution is found on USGS topographic maps at 5 and 10 ft (1.5 and 3 m) contour intervals. These maps were prepared in the 1960's and have only been updated for newly

developed man made structures in the 1980's. The maps are grossly out of date and have an insufficient level of detail for resolving features in centimeter micro-topographic data sets. Exploring higher resolution and accuracy techniques to derive better DEMs is essential.

The original form of the USGS DEM had a spatial resolution of 30 m horizontally, and the RMSE of the vertical accuracy is 7 – 15 meters (USGS, 1993). This effectively makes the vertical accuracy of the USGS DEM obsolete when compared to a RMSE of less than 20 cm resolved in the LIDAR data. For this comparison, the USGS DEM was reprojected from NAD27 UTM coordinates to NAD83 and resampled to 2.5 m resolution using bilinear interpolation. The elevations were converted from feet to meters and then adjusted from NGVD29 to NAVD88 using the NGS VERTCON model. The result was a USGS DEM data set with equal extents and projection as the LIDAR derived dataset for the study area.

A focal mean filter was performed over both maps to smooth interpolations. Subtracting the ATM map from the USGS map produced an elevation residual map (Figure 2.6). Examination of both the ATM derived map and the USGS topographic map reveals an average 2 m elevation difference. From the residual map, the depressions appear to be actually 2 – 3 m deeper than in the USGS DEM. This is an interesting result because it may indicate that the depressions have gotten deeper in the past 40 years when compared to the topographic maps. Alternatively, it may be due to the different methods used for determining the USGS topographic maps. Typically, USGS topographic maps were determined from photogrammetry off aerial stereo photographs. Often, there are trees in the bottom of these depressions and the topographic surface determined from

photogrammetry may actually be in the tree canopy. Since some of the LIDAR pulses can hit the ground in between the trees, these measurements better represent the actual ground surface.

In general, there are two main basins depicted in the lower half of the map and a plateau in the center. The USGS map does not depict the bottom of the basins, as deep as they truly are nor the height of the plateau surface as high as it actually is. The ATM data is a denser set of data points and shows an interpretation closer to reality. The residual map quantifies how the ATM data more accurately depicts the ground surface and effectively preserves detail after being subjected to interpolation, filtering and smoothing. LIDAR technology has shown here to be another useful technique in remote sensing of higher accuracy and detail than that of USGS topographic maps for quantifying landscape topography.

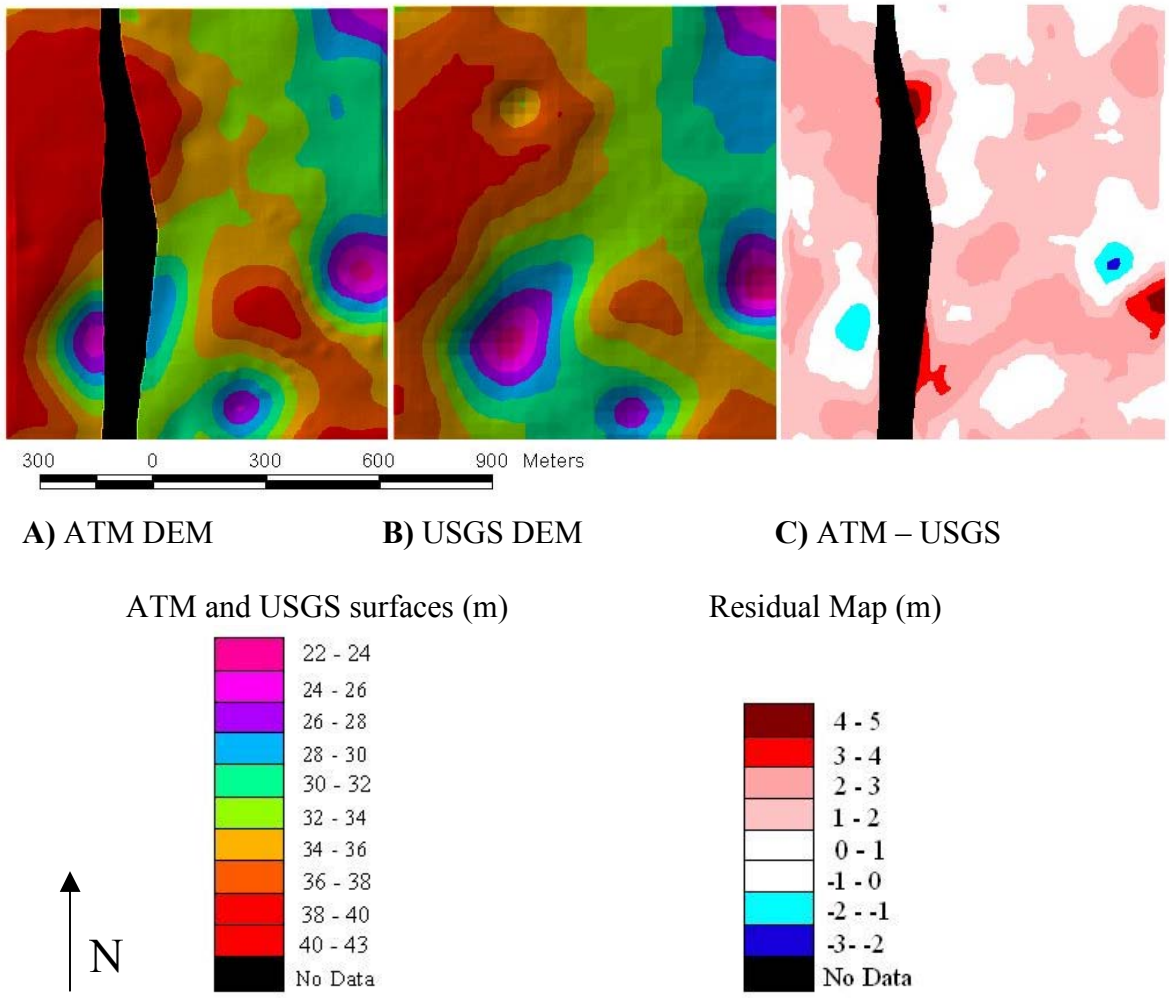

Figure 2.6 Comparison between an ATM derived and USGS derived DEM of the study area. **A)** NASA's ATM data derived DEM. **B)** DEM derived from resampled USGS topographic map. **C)** Residual map of ATM – USGS, red shades are areas of positive elevation difference where land surface is actually higher than depicted in the USGS map and blues indicate negative associations where topography from the USGS map does not resolve accurate depths of features. Color-coded elevation in meters and black indicates no data.

3. Ground Penetrating Radar Studies

3.1 Background

Ground-penetrating radar (GPR) is an active, non-intrusive, high-resolution method for detecting and mapping subsurface geological features *in situ*. It is widely used in geophysical site characterization studies because it allows for excellent documentation of the lateral extent, continuity, depth and thickness of the subsurface units in areas where the soil and shallow strata have low conductivity (Wilson and Beck, 1988). In this study, GPR was utilized to map the subsurface to document and aid in the analysis of target features. A premise of the original hypothesis was that subsurface reflections depicted in the GPR would help to correlate the relationship of subsurface karst processes with surface features. The correlation may help predict incipient sinkhole indicators. The first objective was to determine if the targeted surface features are associated with buried karst structures.

Ground penetrating radar has many successful and diverse applications that include mapping ice thickness, water depth in lakes, bedrock depth, soil stratigraphy, and water table depth. It has been used to delineate rock fabric, detect voids and identify karst features (Davis and Annan, 1989). In Texas, GPR was used to image a collapsed paleocave system and demonstrated its potential utility in 3-D surveys (McMechan et al. 1998). Ground penetrating radar has proven successful in exploring dolines, mapping the surface of the clay layer and mapping sedimentary structures in surficial sediments in covered karst terrains such as central Florida (Church and Webb, 1985). In central Florida, GPR has been an effective hydrogeologic tool used to delineate deep water table

depths, stratigraphy, voids and paleo-sinkholes for land application sites (Stangland and Kou, 1987). Personnel at the U.S. Army Engineer Waterways Experiment Station used GPR to delineate karst topography and cavity features just north of Ocala, Florida. They found several prominent anomalies in areas where there were no surface indicators of cavities and then used drilling to verify the existence of the cavities to be true (Cooper and Ballard, 1988). Other GPR studies range from soil stability at the Walt Disney World theme park in Orlando, FL, to mapping the configuration of the top of bedrock in Lake County, Florida and to geophysical site characterizations in northwestern Orange County, Florida. When active, the Florida Sinkhole Research Institute personnel used GPR to locate potential sites of sinkhole development near Gainesville in Alachua County, Florida (Stangland and Kou, 1987, Wilson and Beck, 1988).

The GPR system operates by transmitting brief electromagnetic pulses from an antenna into the ground. Radar waves are able to propagate through electrically resistive earth materials, such as quartz sand and limestone. Changes in conductivity or electrical properties between different layers or from buried objects cause the radar pulse to be reflected. Between transmission pulses, the antenna also acts as a receiver recording the reflected signals and measuring the length of time between the pulse and its returned reflection. The return time is measured as two-way travel time (twtt) and is proportional to the depth of the reflector (Stangland and Kuo, 1987; Cooper and Ballard, 1988; Wilson and Beck, 1988; Davis and Annan, 1989; Mellet, 1990). As seen in Figures 3.1a – 3.8a, the reflected signals are plotted as black bands on the scan-line graphic recorder. The upper two bars on the radar profiles are the transmit pulse which is a direct transmission from the antenna. The next three bars are the ground surface reflection. The top of the

solid bar represents ground surface (the second solid bar below the top of the profile) (Wilson, 1998). The elapsed time (from when the transmitted pulse ended until the reflection was received) is measured in nanoseconds (ns), and is displayed on the vertical axis of the profiles as depth in meters.

3.2 GPR Data Collected

The GPR survey for this project was completed in the summer of 1999 at the study site in Apopka, Florida. The equipment used was the Subsurface Interface Radar System (SIR-3) by Geophysical Survey Systems, Inc. The GPR data was collected with a control unit/profiling recorder using a 100 MHz antenna provided by William Wilson of Subsurface Evaluations Inc., (SEI) in Tampa, Florida. The position of the GPR transects were determined by the surficial features to obtain cross-sections below ground. By pulling the antenna behind a truck across the ground, a continuous cross-section of the subsurface along the predetermined transects was attained.

Eight exploratory transects were collected ranging in length from 183 m to 427 m. The transects were labeled A through H corresponding to the ETS survey lines that crossed the targets above ground (Figure 2.4). Profiles A and B have a scanline length (interchangeable with twtt) of 408 ns and profiles C – H have a twtt of 510 ns. The vertical scales of the GPR are estimated based on the known two-way travel time (twtt) velocities of the radar signal in subsurface materials similar to those at the study site (Table 3.1). Based on this and the experience of Subsurface Evaluations Inc., a twtt velocity of 4ns/ft propagation rate was assumed for the dry quartz sand and converted to 13.12 ns/m. Assuming dry sandy soil, profiles A and B have a maximum depth of scanning of approximately 27.5 m (Figures 3.1a and 3.2a).

Table 3.1 Two-Way Travel Time Velocities for Subsurface Materials in the central Florida, Orlando region (Adapted from Mellet, 1990; Wilson, 1998).

Material	**Standard Two-Way-Travel-Time Velocities**
Unsaturated quartz sand	0.25 ft/ns (4 ns/ft propagation rate)
Unsaturated clayey or silty soil	0.17 ft/ns (6 ns/ft propagation rate)
Water-saturated materials	0.09 ft/ns (11 ns/ft propagation rate)
Water	0.056 ft/ns (18 ns/ft propagation rate)

Material	**Approximate Vertical Depth Scales for Study GPR profiles**
Unsaturated surficial sands	1 inch : 15 ft (~4.5 m)
Unsaturated clayey or silt soils	1 inch : 10 ft (~3.0 m)
Water-saturated materials	1 inch : 5.5 ft (~1.6 m)

Six out of eight profiles were scanned at 510 ns (vertical time scale: 8.5 inches per 510 ns or 1 inch per 60 ns). The velocities and vertical depth scales recommended by William Wilson, P.G., Principal Geologist and President of Subsurface Evaluations, Inc. (SEI), Tampa, Florida.

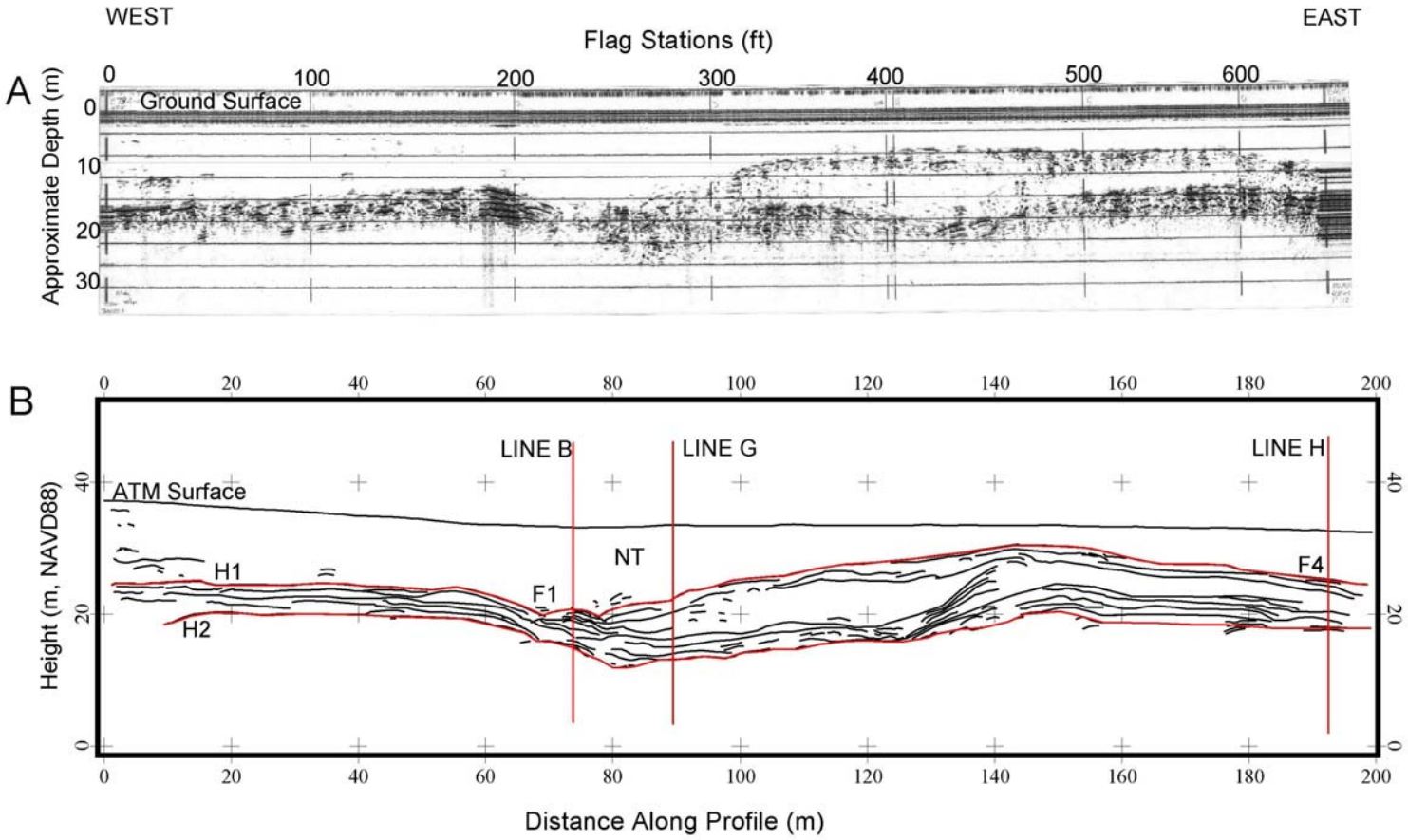

Figure 3.1 Transect A. **A:** GPR raw radar profile from west to east with flag stations in ft. and estimated depth below ground in meters. **B:** Line drawing interpretation of GPR profile. The red lines are the interpreted horizons H1 and H2. The north trough (NT) is shown going into the page and feature one (F1) is the karst feature within the sediment layers.

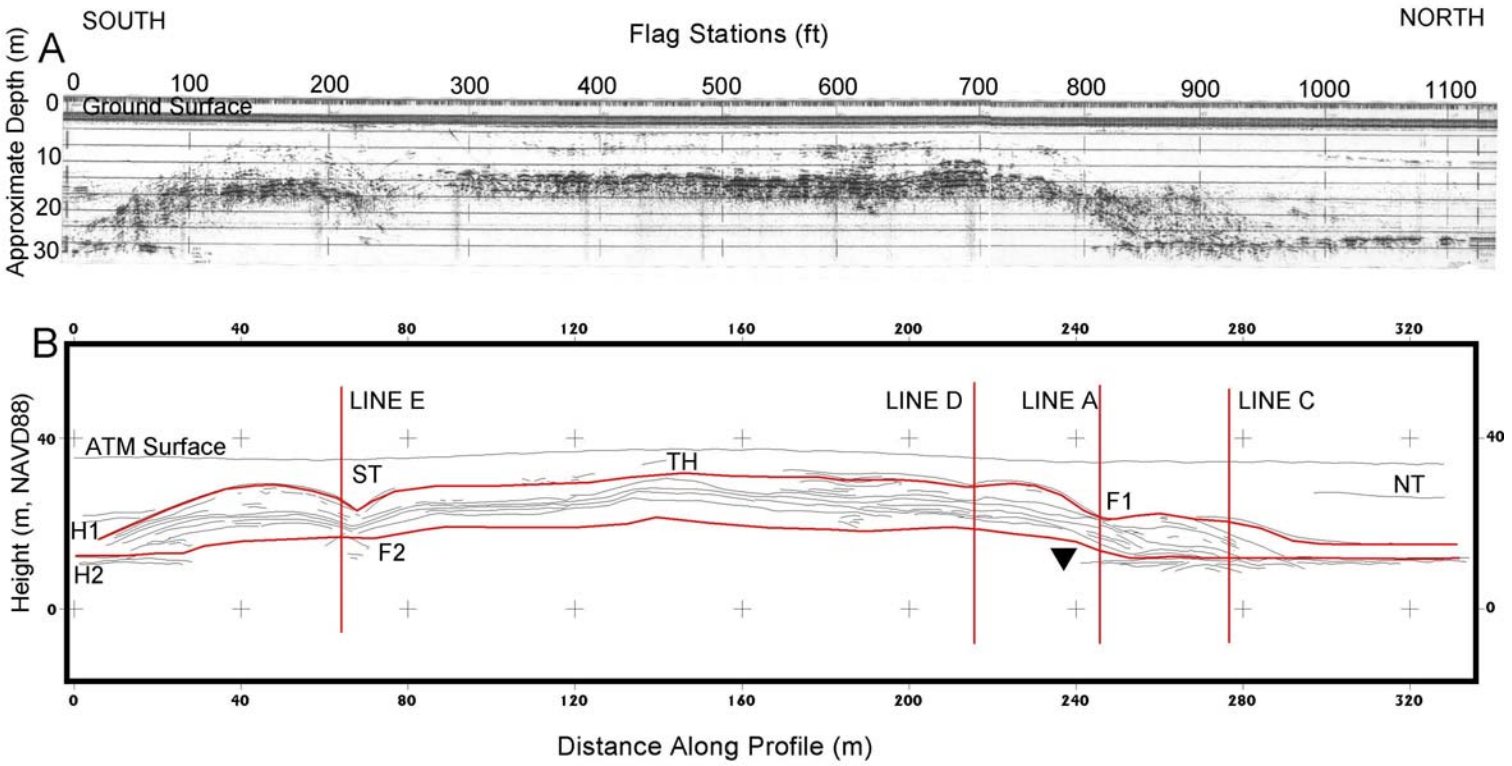

Figure 3.2 Transect B. **A:** GPR raw radar profile from south to north with flag stations in ft. and estimated depth below ground in meters. **B:** Line drawing interpretation of GPR profile. The red lines are the interpreted horizons H1 and H2. The north trough and south trough (NT, ST) are shown going into the page. The topographic high (TH) is in the center and features one and two (F1, F2) are the karst features within the sediment layers. The water table is shown by the upside down triangle symbol.

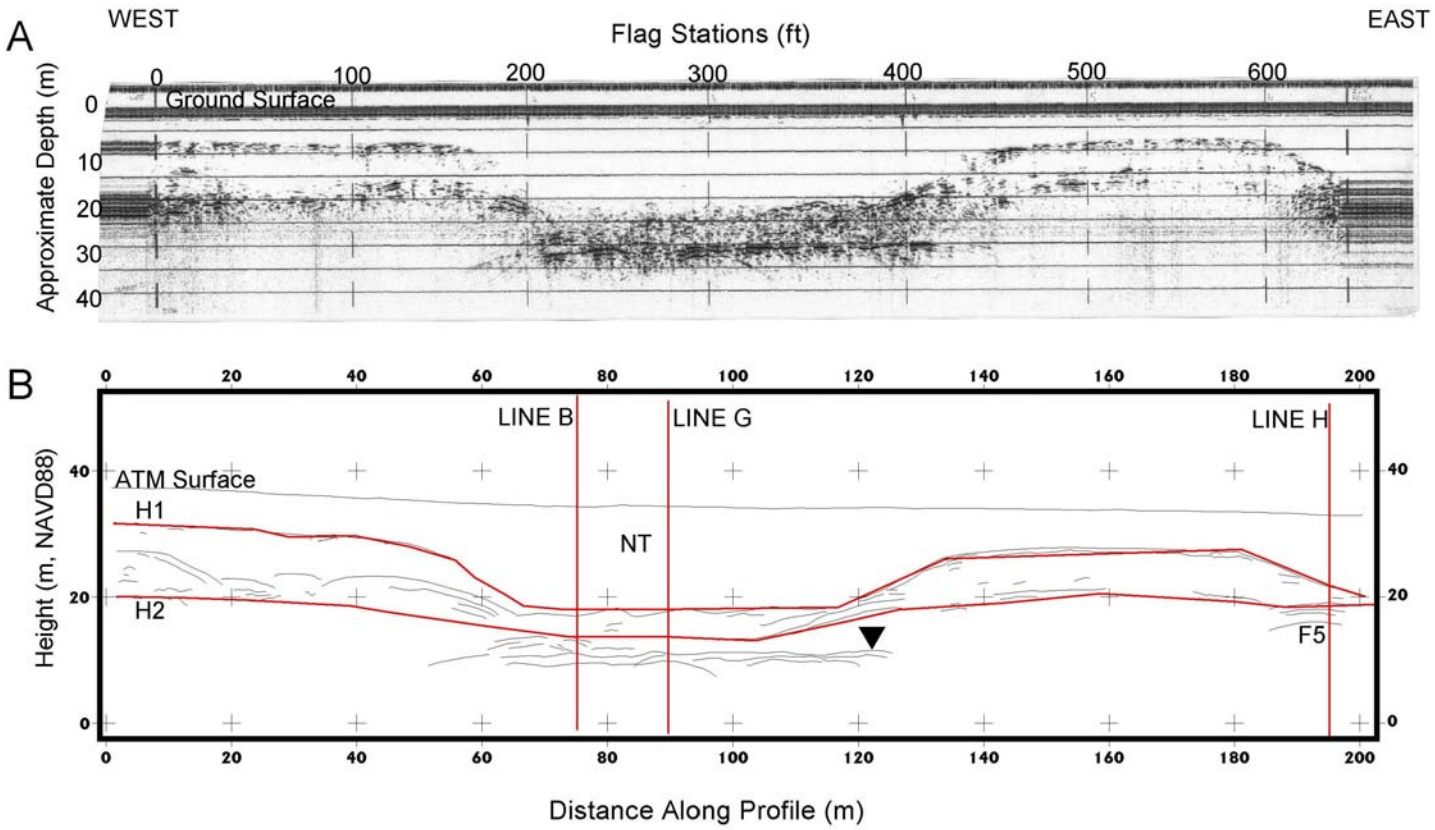

Figure 3.3 Transect C. **A:** GPR raw radar profile from west to east with flag stations in ft. and estimated depth below ground in meters. **B:** Line drawing interpretation of GPR profile. The red lines are the interpreted horizons H1 and H2. The north trough (NT) is shown going into the page. The water table is shown by the upside down triangle symbol.

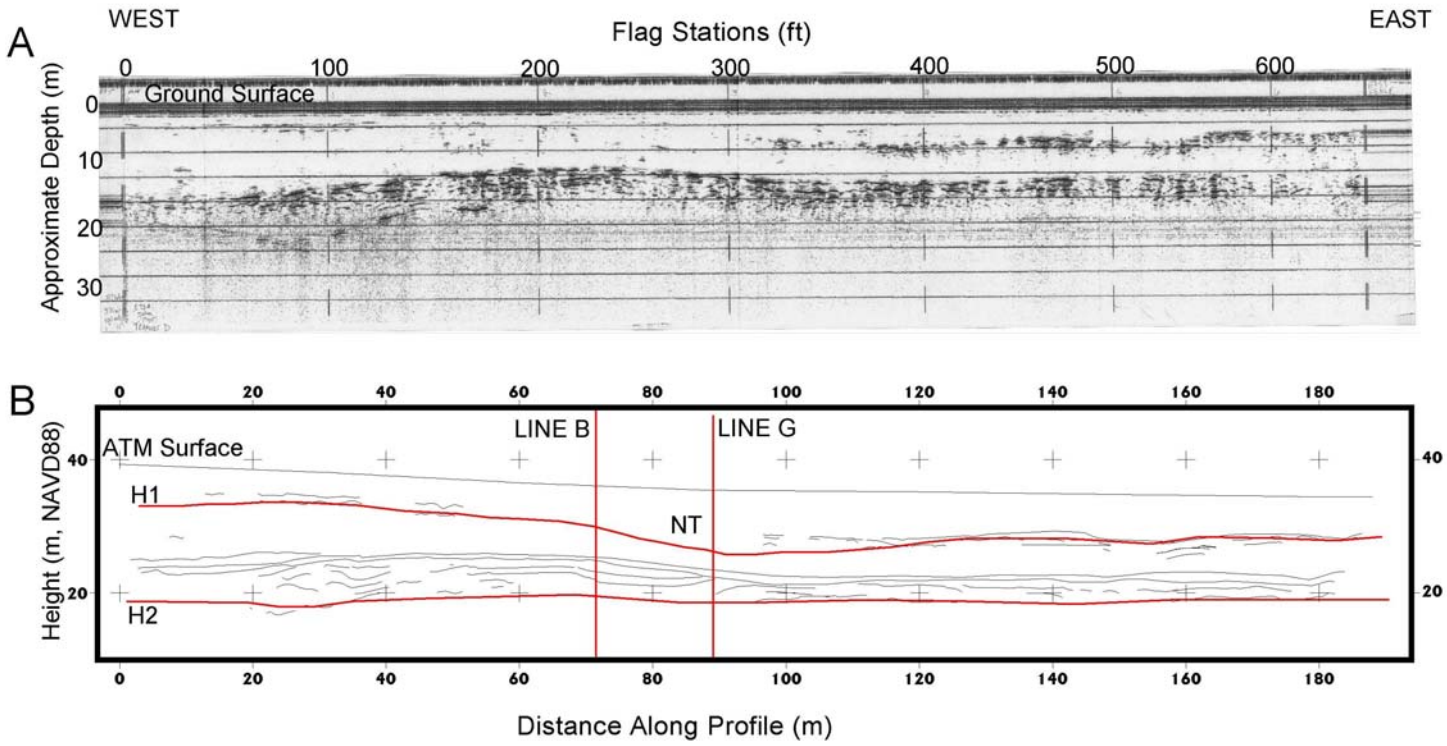

Figure 3.4 Transect D. **A:** GPR raw radar profile from west to east with flag stations in ft. and estimated depth below ground in meters. **B:** Line drawing interpretation of GPR profile. The red lines are the interpreted horizons H1 and H2. The north trough (NT) is shown going into the page.

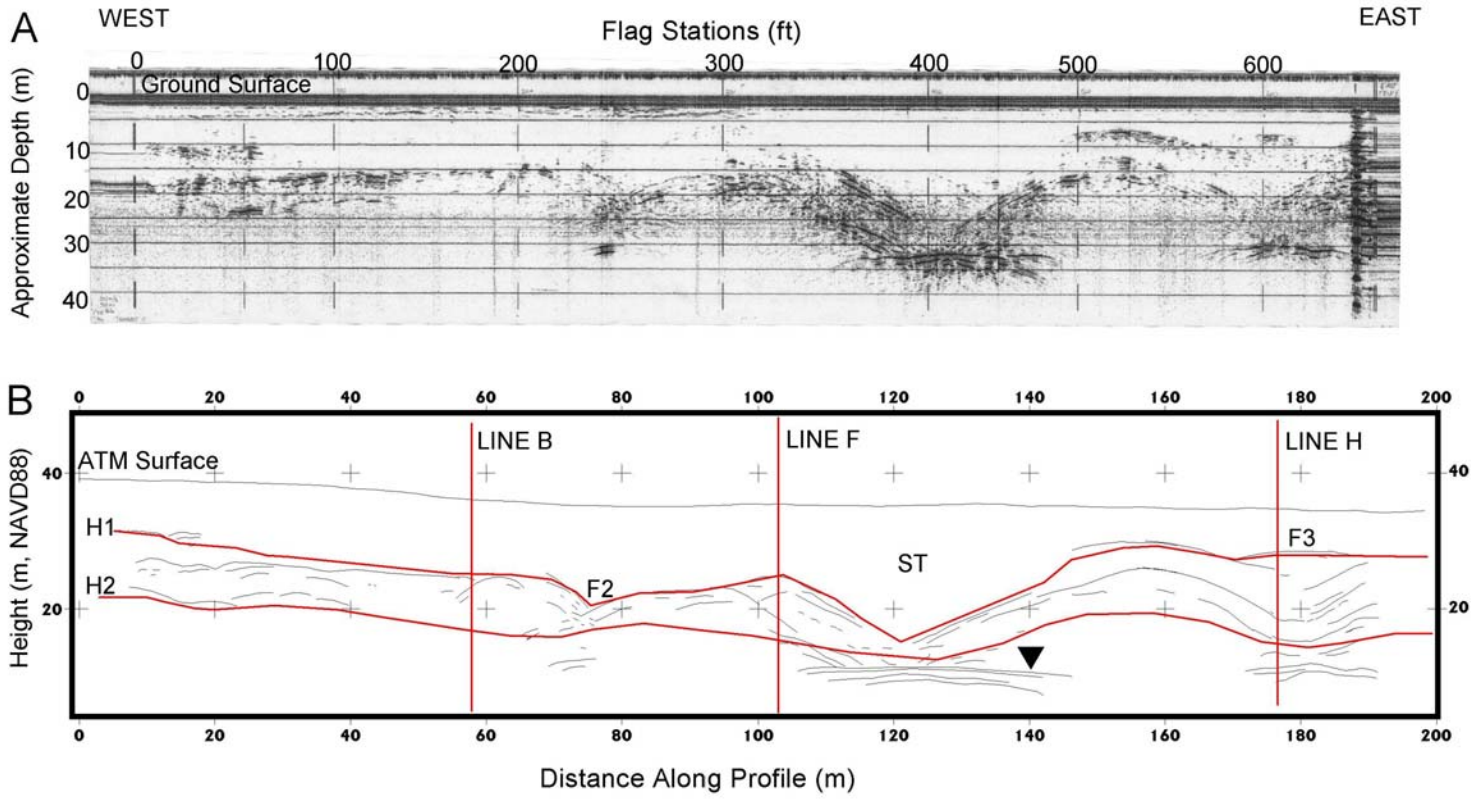

Figure 3.5 Transect E. **A:** GPR raw radar profile from west to east with flag stations in ft. and estimated depth below ground in meters. **B:** Line drawing interpretation of GPR profile. The red lines are the interpreted horizons H1 and H2. The south trough (ST) is shown going into the page and features two and three (F2 and F3) are the karst features within the sediment layers. The water table is shown by the upside down triangle symbol.

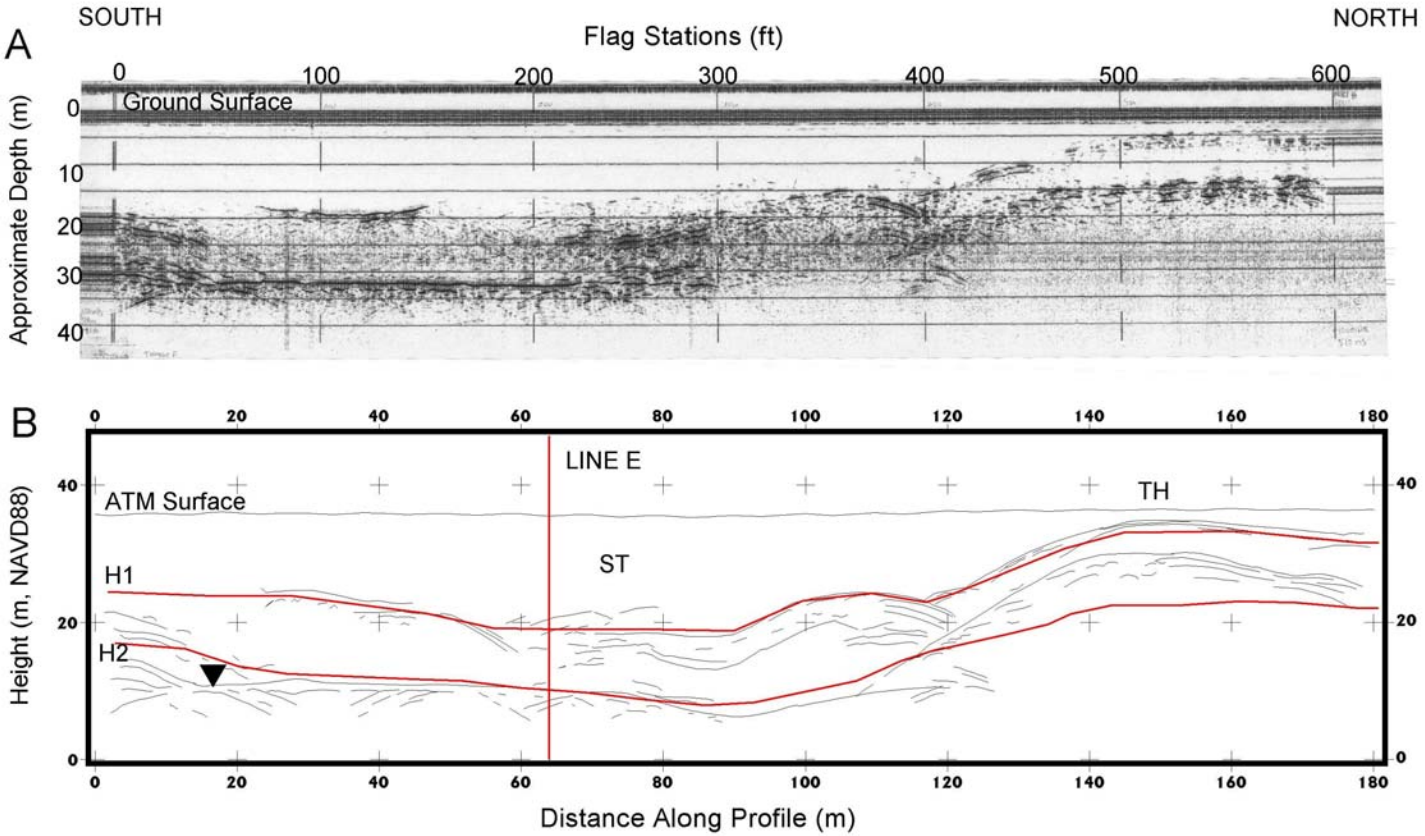

Figure 3.6 Transect F. **A:** GPR raw radar profile from south to north with flag stations in ft. and estimated depth below ground in meters. **B:** Line drawing interpretation of GPR profile. The red lines are the interpreted horizons H1 and H2. The south trough (ST) is shown going into the page and the topographic high (TH) is on the upper right side. The water table is shown by the upside down triangle symbol.

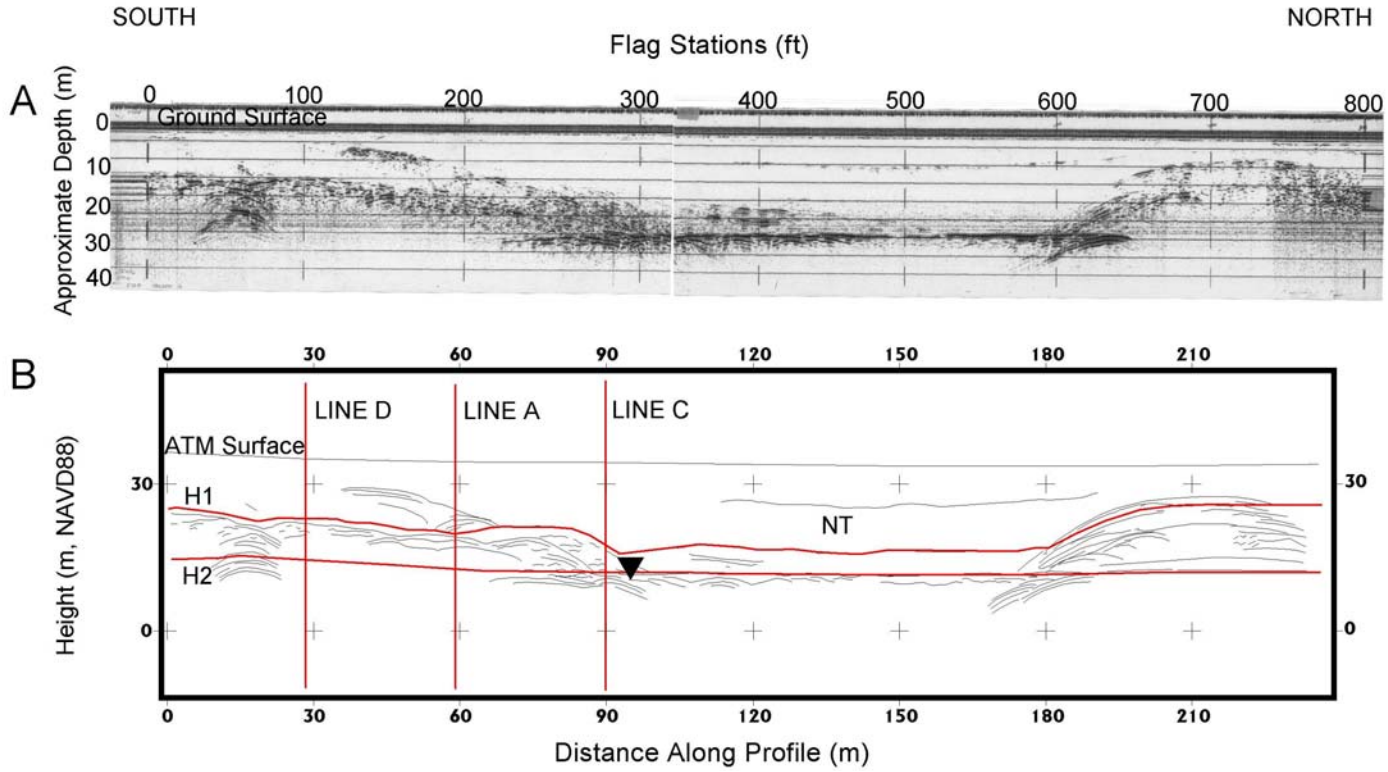

Figure 3.7 Transect G. **A:** GPR raw radar profile from south to north with flag stations in ft. and estimated depth below ground in meters. **B:** Line drawing interpretation of GPR profile. The red lines are the interpreted horizons H1 and H2. The north trough (NT) is shown going into the page. The water table is shown by the upside down triangle symbol.

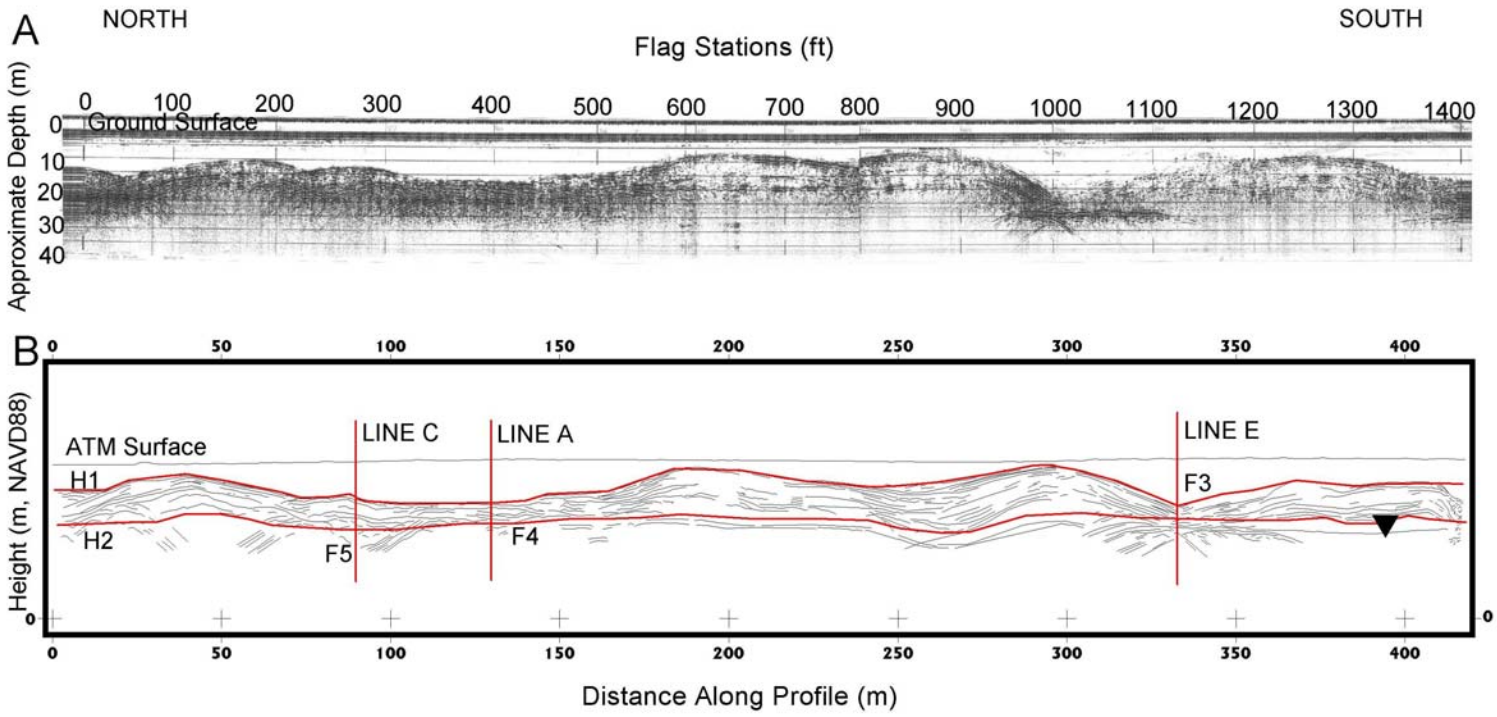

Figure 3.8 Transect H. **A:** GPR raw radar profile from north to south with flag stations in ft. and estimated depth below ground in meters. **B:** Line drawing interpretation of GPR profile. The red lines are the interpreted horizons H1 and H2. Smaller scale features three, four and five (F3, F4, and F5) lie within the sediment layers of this transect. The water table is shown by the upside down triangle symbol.

The profiles C-H have a maximum attainable depth of approximately 35 m (Figures 3.3a – 3.8a). The radar profiles provided reflections of the subsurface structures and sediment boundaries. The profiles show the variable thickness Plio-Pleistocene unconsolidated clastic sediments in this area that overlie cavernous Eocene limestone (Table 1.1). According to a site well log completed for the City of Apopka (Boyle Engineering Corporation, 1997), the limestone at this location is approximately 110 to 150 ft (34 and 46 m) below land surface. The acquired reflections had a maximum depth of 30.5 m or approximately 100 ft. below land surface. Therefore, in this study, depth to the limestone was never imaged. Instead, what we believe the profiles depict is the response of the sediments to the dissolution of the underlying limestone.

A problem with using GPR data is that of an inherent limitation to all surface geophysical methods is the decrease in resolution with increasing depth (Benson and Yuhr, 1993). The actual depth of scanning is somewhat less due to clayey soils, water-saturated sands, or if the signal was absorbed by other electrically conductive materials. Electrically conductive materials, such as clay, and water rapidly absorb the radar waves and limit radar penetration. This is due to the electrical properties of geologic material primarily being controlled by their water content (Topp et al., 1980; Davis and Annan, 1989; and Wilson, 1998). In short, the penetration capability of GPR is dependent on the frequency of the antenna and the electrical properties of the earth materials involved (Stangland and Kuo, 1987). It is known that the overlying clay and clayey-sediments in this area may absorb the signal, decreasing penetration depth (Wilson and Beck, 1988),

which may prohibit the radar pulse return of some buried features as well as the underlying limestone because the sediments absorb the signal.

A second problem that arises in GPR data collection is the difficulty to maintain a constant speed while pulling the antenna behind a vehicle. Variability in the speed of the antenna may cause the horizontal scales on the profile to skew. This problem was controlled by marking the profiles during collection with vertical dashed lines that corresponded to the 100 ft (30 m) interval flagged stations at the surface whose coordinates were surveyed with the total station.

3.3 Interpretation

To best use the distance and depth data along the GPR profiles and use the data to correlate the surface expressions, the reflected radar signals had to be spatially corrected. To do this, the profiles were traced onto Mylar paper and digitized using the ArcInfo GIS software package. Each profile was then converted into a digital line drawing representation. To correct for the horizontal error that occurs from towing the antenna over the ground, we used surface control points (the surveyed flag stations) to spatially adjust the line drawings into actual study site coordinates. This technique is similar to rubber sheeting which uses the horizontal control points along with the assumed velocity to transform the profiles into distance-depth cross-sections (Figures 3.1b - 3.8b). The velocities and the vertical depth scales presented are thought to be reasonable (Table 3.1) and the details of the GPR survey are presented in Table 3.2.

Table 3.2 Details of Study GPR Survey Transects

Transect	Length (m)	Trend	TWTT (ns)	Conversion (m)	Max Depth (m)
A	199	W – E	408	1 inch = 3.6	25.2 (~83 ft)
B	328	S – N	408	1 inch = 3.6	31.5 (~103 ft)
C	200	W – E	510	1inch = 4.5	31.5 (~103 ft)
D	198	W – E	510	1inch = 4.5	27.0 (~89 ft)
E	182	W – E	510	1inch = 4.5	31.5 (~103 ft)
F	180	S – N	510	1inch = 4.5	32.0 (~105 ft)
G	238	S – N	510	1inch = 4.5	31.5 (~103 ft)
H	418	N - S	510	1inch = 4.5	31.5 (~103 ft)

Maximum depth obtained estimated from 13.12 ns/m. The scan line length is interchangeable with two-way travel time (TWTT).

The radar profiles all have two main features in common, a top transparent zone and a zone of layered reflections. These zones are interpreted to represent respectively a zone of siliciclastic sediments and a zone of clay and clayey-sands. Horizon 1 (H1) and horizon 2 (H2) represent the top and bottom boundaries of the clayey soil zone. This unit is laterally extensive with intermittent groups of gentle subsurface reflections. H1 corresponds to the base of a generally transparent zone on the sections and is interpreted as the top of the clay-rich layer that is underlying a unit of sandy surficial soils and sand. H2 corresponds to the deeper bottom boundary of the reflections. This represents the bottom of a gradational contact between the inferred subsurface unit of clay-rich sand and a deeper unit of unconsolidated sands and clay.

The clay rich layer varies from 4 – 15 m in thickness and confidence decreases outward, as computer interpolation of the surfaces increases from the control points. In profiles B, C, and E - H the signal is interpreted to be completely absorbed by the water table as indicated in Figures 3.2b, 3.3b and 3.5b – 3.8b, respectively. Water tables in many karst areas are almost flat owing to the high hydraulic conductivity (Fetter, 1994) and for our purposes this horizon was not used in the analysis. The reflections, or inferred soils layers, demonstrate lateral continuity across most of the survey site and the data is well constrained at the coincident surveyed points.

The shallower of the two reflective interfaces, H1, displays good lateral continuity and returned after an elapsed time of approximately 90 to 180 ns, or a depth of approximately 4 -15 m below the surface. The lower interface of this unit, H2, also displays good lateral continuity within all transects and typically returned after an elapsed time of approximately 180 to 280 ns or an elevation of approximately 25 to 30 m below ground.

Within the interpreted horizons H1 and H2, there are three main features within the profiles, two swale or trough like karst depressions termed north trough (NT) and south trough (ST) for their locations within the study site. There is also a topographic high (TH) in center area of the study site seen in transects B and F (Figures 3.2b and 3.6b). The layered clayey sediment ranges in thickness from 5 to 15 meters and is approximately 15 meters below the land surface. Figures 3.1b and 3.3b show examples of where H2 separates in places into two packages that are more complicated.

At the northern end of the study site lies the north trough (NT) that is intersected by transects A – D and G (Figures 3.1b – 3.4b and 3.7b). Specifically, Figure 3.3a is a

clear representation of NT. The north trough has a vertical relief of approximately 12 m and trends north to south for approximately 140 m. In the southern portion of the site, transect E, (Figure 3.5b) between stations 300 and 500, crosses the full extent of the southern trough (ST) and is intersected by transects B, F, and H (Figures 3.2b, 3.6b and 3.8b). ST has approximately 10 – 15 meters of vertical relief and is approximately 100m wide.

Within the complicated strata above H2 there are five smaller individual features that lie within or are in close proximity to the main trough features NT and ST and are thought to be subsidence or sinkhole features. Incipient subsidence, dolines and sinkhole type karst features are known to produce a bow tie or V- shape reflection on GPR profiles (Wilson and Beck, 1988; Wilson, 1998). Upward pointing hyperbolic reflection patterns may represent a soil ravelling and/or lateral reflections from the sand and clay interface (Beck, 1986; Wilson and Beck, 1988) and horizontal sediments or the water table produce laterally continuous, flat reflections (Fetter, 1994). In the northern trough-like feature (NT), bound by the horizons at the intersection of transects A and B there is a downwarping of the sediment layers that seem to represent a smaller karst structure termed feature one (F1) between the flagged stations 200 and 300 (Figures 3.1a and 3.2a). Specifically, at station 400 in Figure 3.5a, there is an excellent example of the classic bow tie reflection or V-shaped reflection that Wilson and Beck describe as indicative of buried karst features in their well known 1988 paper. This type reflection is indicative of subsidence (or possibly a sinkhole) with sediment filled basin most likely of clayey-sands. The feature in profile F, Figure 3.6a at station 400, and the feature in profile G in Figure 3.7a between flag stations 0 and 100 are smaller examples of the

upward pointing hyperbolic reflections that correlate spatially with edges of the NT and ST respectively, which may be a reflection of the raveling clay sediments here.

Within ST in Figure 3.2a and b, just passed station 200 on transect B there is another bow tie feature, F2. Along transect H, (Figure 3.8a and b) there are three features F3, F4 and F5 depicting or representing downwarping sediments. F3 is intersected in transect E, Figure 3.5b at station 600 and the smaller features F4 and F5 are crossed by transects A and C respectively, just past station 600 on both (Figures 3.1a and 3.3a). These features are good examples of erosional or buried features within the clay rich layer.

4. Direct Comparisons of Surface and Subsurface Topography

4.1 Surface Construction

In order to compare the GPR profiles with spatial features seen in the LIDAR data, the horizons and other features identified in the GPR data need to be presented in a planar (map) form. First, the map positions of the profile lines were combined with the lines and horizons digitized off of the two-dimensional profiles. This produced a set of three-dimensional line vectors (Figures 3.1 – 3.8). The procedure was performed for both the line drawing segments and the interpreted horizons, H1 and H2. This transformation allowed the line vectors to be displayed in the form of a 3-D fence diagram constructed within the Arcview 3d Analyst GIS environment (Figure 4.1). While this environment allowed direct comparison of the GPR features with the LIDAR derived surface, interpretation was difficult because of the complex shapes of the subsurface interfaces and the complexity of the 3-D figures themselves.

In order to more easily evaluate the relationships between the topography and the subsurface horizons, the 3-D horizon vectors, H1 and H2, were used to construct continuous 3-D surfaces. The verticies of each horizon were used to define Triangular Irregular Network (TIN) surfaces (Figure 4.2). Unfortunately, the TIN method often produces sharp angular artifacts which form unrealistic surfaces that may be misinterpreted. To produce maps that give a more effective visualization of the surfaces, the TIN surfaces needed to be smoothed.

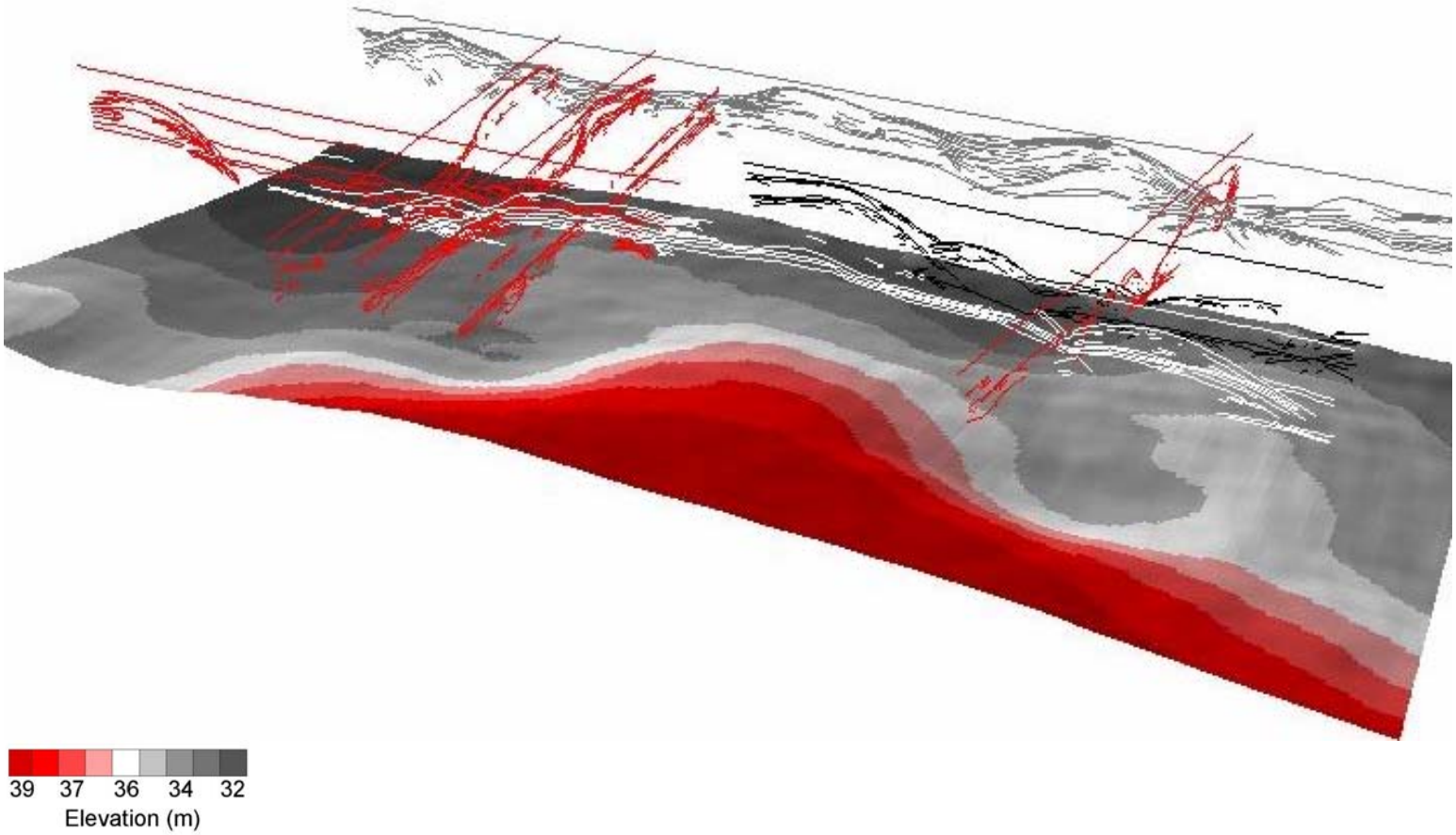

Figure 4.1 3-D fence diagram of the digitized line drawings. The profile line drawings are floating over the LIDAR surface to enhance visualization. The surface is vertically exaggerated by a value of 5 and shaded to enhance the features. Lines A, C, D, E, and G are in red, line B is in white, line F is in black and line H is in gray for visualization purposes. The surface elevations are in meters NAVD88. The view is east northeast.

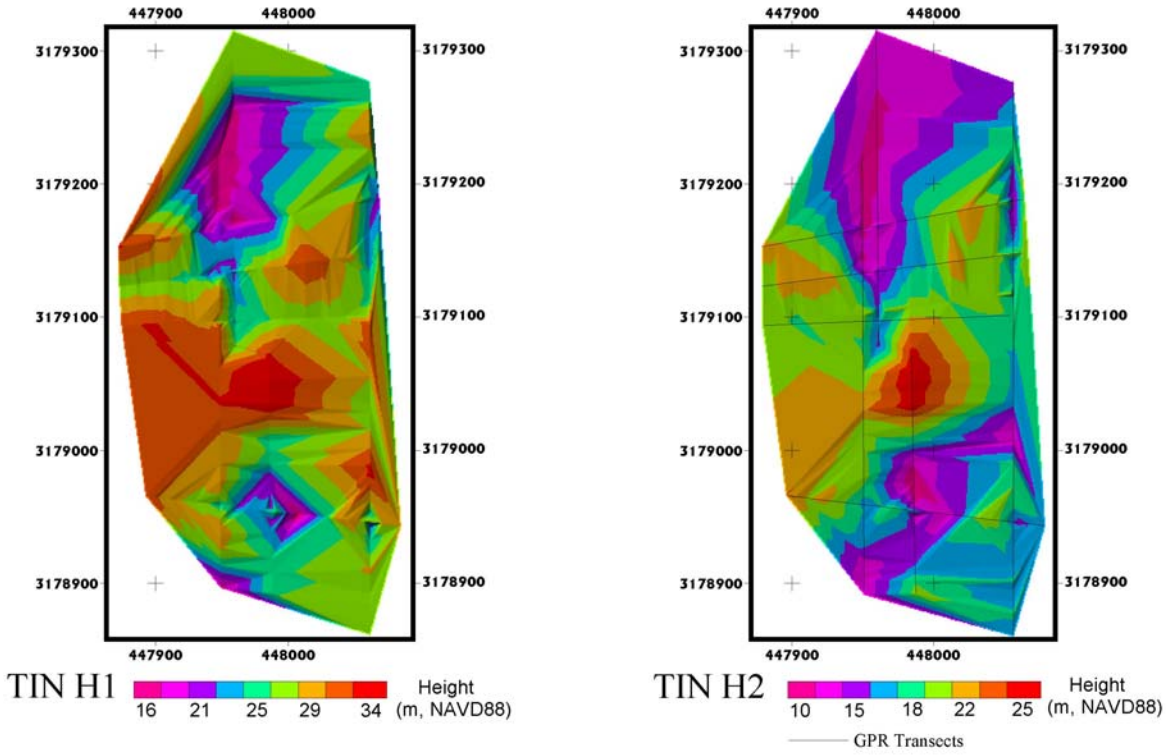

Figure 4.2 Triangular Irregular Network (TIN) surfaces of H1 and H2. The GPR transects are superimposed on H2. Using the TIN method produces sharp angular artifacts that alone are difficult to use in comparison with the LIDAR topographic surfaces.

Smoothing was performed by interpolating the TIN onto a regularly spaced, 1 m, raster grid and applying a low pass filter. The filter used was a focal mean filter which applied an 11 m rectangular moving window to the surface. This 11 m window size was chosen for its capability to smooth the gridded surfaces into a more suitable depiction of the true study site topography for comparison (Figure 4.3). From here, the smoothed surfaces were also contoured to show possible associations between the surface and subsurface topgraphy differently (Figure 4.4). The contour elevations are the same as the surfaces ranging from 32.5 m to 39 m NAVD88.

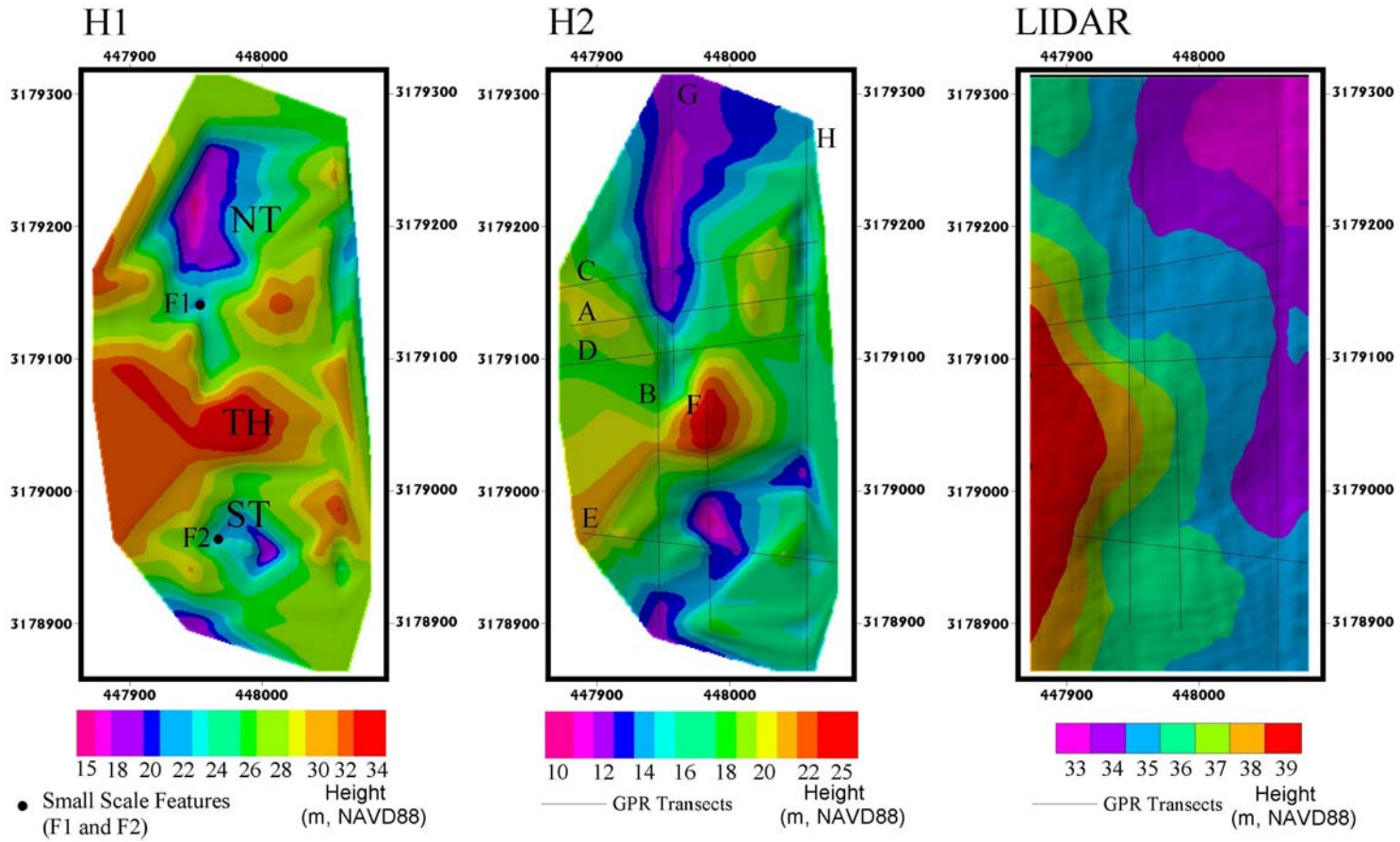

Figure 4.3 Three-panel comparison of the surfaces H1, H2 and the LIDAR topography. On surface H1, the large-scale features (NT, ST, and TH) and the small-scale features, as points, (F1 and F2) are shown. Superimposed on surface H2 and the LIDAR topography is the location of the GPR transects. Measured grid tick interval is 100 m.

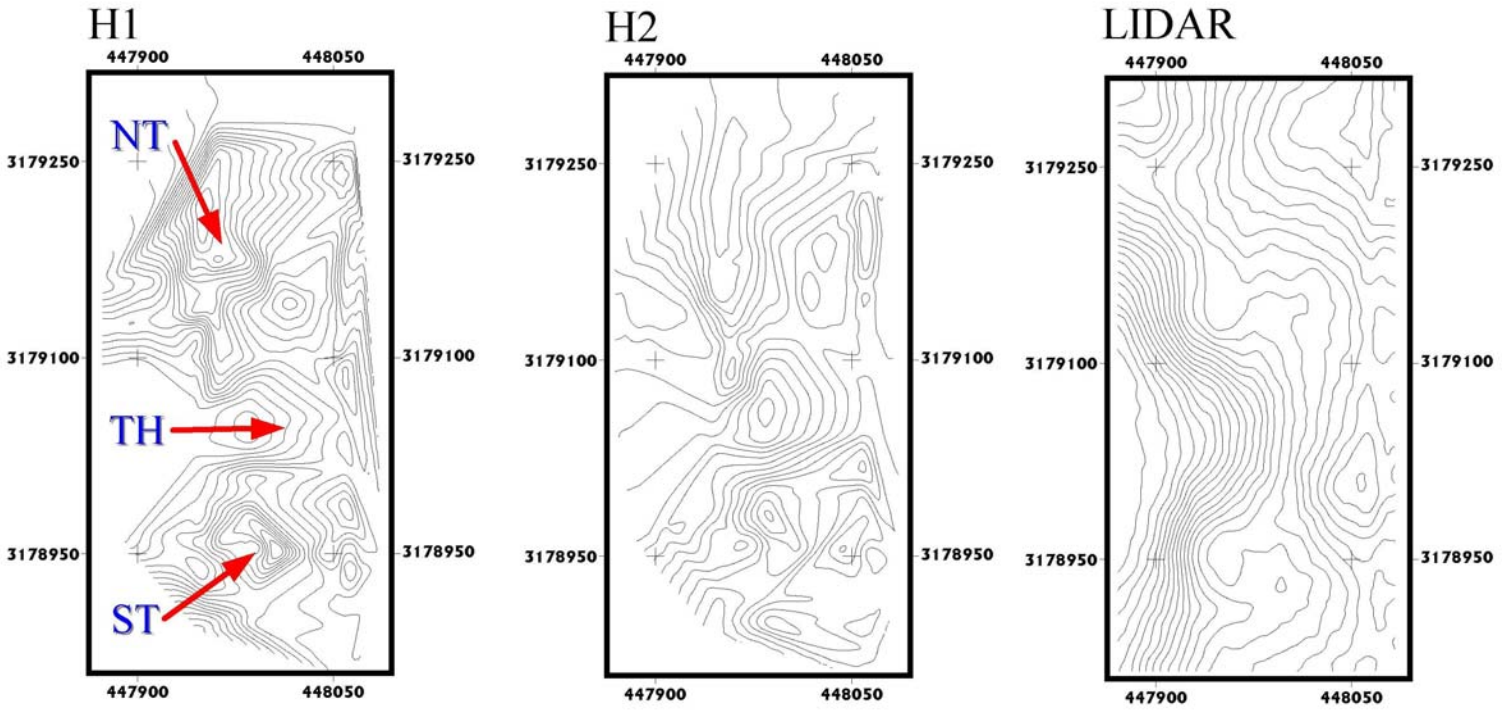

Figure 4.4 Contoured surfaces comparing H1, H2 and the topography derived from LIDAR. On surface H1, the locations of the large-scale features NT, ST, and TH are given. The contour interval depicted is 2 m produced from 1 m cell size grids and smoothed using an 11 m size low pass filter. Measured grid tick interval is 100 m.

4.2 Observations

The LIDAR derived topography is compared to the two surfaces interpreted as being H1 and H2, described previously in chapter 3 as the base of the transparent zone and the bottom of a clay rich layer, respectively. Both the H1 and H2 surfaces contain three significant features that correlate with three similar features on the surface topography. These are two troughs, one in the northern section of the site and one in the southern section and an area of high elevation in the center.

The troughs are inferred from the GPR profiles to be large-scale depressions associated with karst development below the surface. In the northern portion of the site, the North Trough (NT) is approximately 140 m long, 50 m wide with 12 m of vertical relief varying from 10 – 30 m below the ground surface (Figure 4.3). The second trough trends south from the southern edge of the topographic high area. The South Trough (ST) extends approximately 70 m long and 50 m wide with 10 – 15 m of relief also 10 – 30 m below the surface (Figure 4.3). A 75 m long area of topographic high (TH) elevation divides the two troughs and is located nearly center in the study site (Figure 4.3). From the constructed surfaces, H1, H2 and the LIDAR topography there is a clear association among the troughs and the area of topographic high elevation between the surfaces.

There are also interesting differences among the features and between the surfaces themselves. For example, on the radar profiles the bottom of NT is approximately 30 m below the surface and ST is around 15 m below the surface (Figure 3.2). NT is also much larger than ST and more elongated. This difference can be seen in Figures 4.3 and 4.4, the elongation of NT in H2 may be exaggerated due to a lack of control in the NW

portion of the study area. Between the individual surfaces, NT varies from H1 at about 10 m below the surface to approximately 30 m below the surface in H2. ST is also 75 m wider in the lower surface H2 than in H1 (Figure 4.3). In contrast, the area of higher elevation (TH) does not change very much but does appear to be steeper in H2 when compared in the two surfaces.

The study site was chosen from target features visualized in the LIDAR data and discused in chapter 2 (Figure 2.3). When compared to the subsurfaces H1 and H2, NT is spatially associated with a subtle surface drainage feature that is offset to the northeast, it is approximately 140 m wide and 200 m long with less than one meter of relief (Figures 2.4, 4.3 and 4.4). NT sits just above three of the targeted features on the north side of the topographic high and to the south of this ST is directly below the other target feature (Figure 4.3). TH is also observed within all of the surfaces. In order to accurately compare the derived surfaces from the GPR data that were filtered, the low pass filter also had to be applied to the LIDAR derived surface. This further smoothing of the topography eliminates detail that shows what was being attempted in this study. The LIDAR derived surface in Figure 2.4 was constructed prior to the need for further smoothing and thus this surface better exemplifies the semi-closed depressions that lie above ST.

Within the large-scale features, NT and ST, small-scale features were identified within the clayey layer from the GPR profiles, these can also be correlated with the surface topography. The small-scale features are depicted as points in Figure 4.3. Feature F1, is approximately 16 m below the surface is 34 m wide and has 5 meters of vertical relief (Figures 3.1 and 3.2).

Feature 2 is close to 18 m below the surface, it is 17 m wide also with 5 m of vertical relief (Figures3.2 and 3.5). The similarity in the depth and relief between F1 and F2 is interesting and that F2 is half as wide as F1 follows the pattern of the southern trough being generally much smaller than the trough to its north. There were a total of five smaller features observed in the radar profiles however for this comparison only F1 and F2 were used.

A plausible cause for the correlation of surficial troughs and subsurface features may be explained by the draining down and out of surficial materials through pre-existing karst features. The concept is that surficial sediments are gradually draining or raveling down predetermined pathways which may be buried karst features. The elongated nature of NT and the subtle surficial trough above at the surface is a good example of a favored flow path (Figure 4.3). A flow direction diagram was constructed using vectors derived from the eleavtion differences in the surface (Figure 4.5). This vector map illustrates the direction and magnitude of flow in the study site topography. Note the similar correlations with the locations of NT and ST from Figure 4.4.

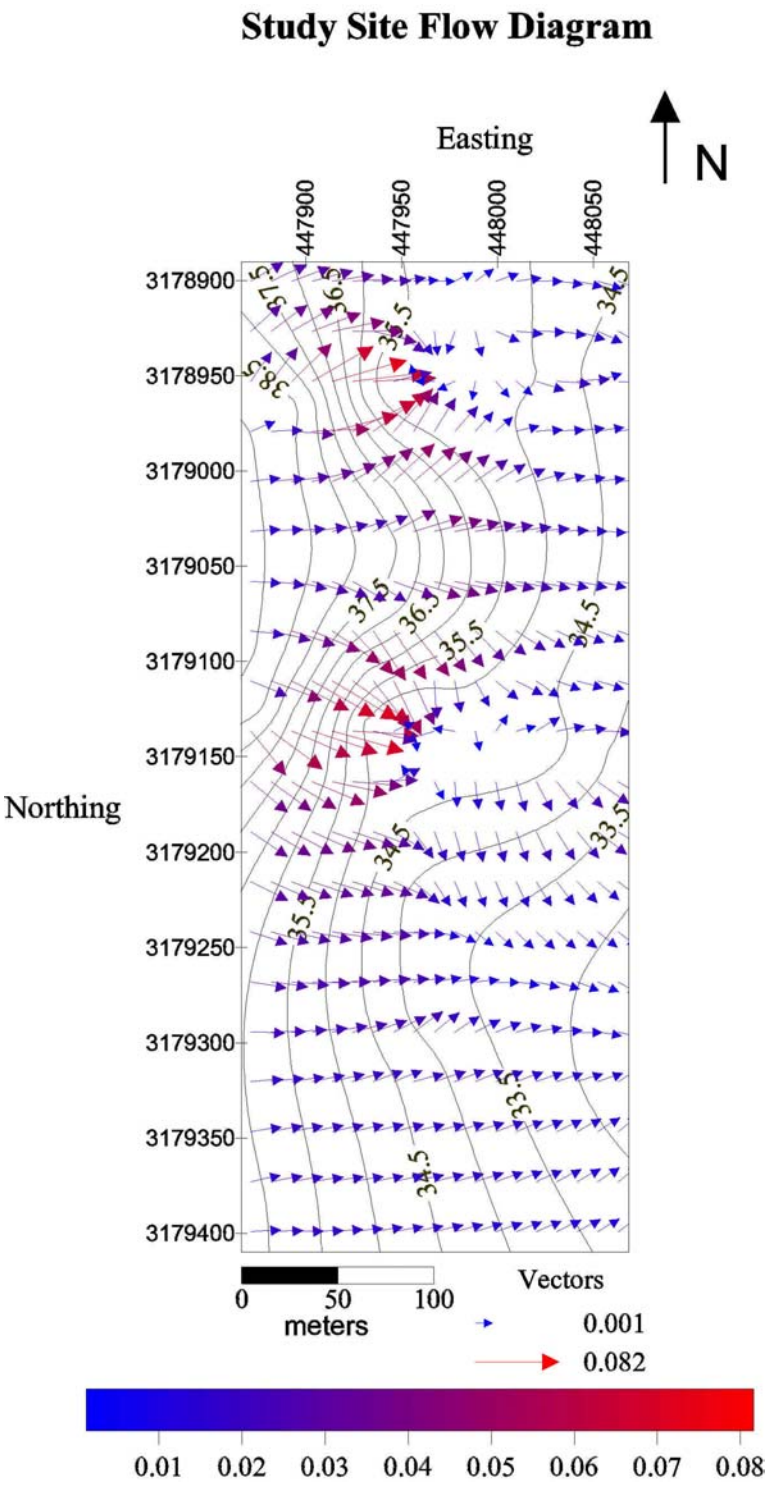

Figure 4.5 A vector diagram of the direction of flow or drainage at the study site from the LIDAR derived DEM. ***Note:*** Where the vectors converge and increase in magnitude is on top of NT and ST. The vector size increases and the color shifts with magnitude from blue through to red.

The feasiblity of surficial features being a result of karst structures below is further demonstrated by the sinkhole type feature F1, which is 34 m large and lies within the clay-rich layer below the NT (Figures 3.1, 3.2 and 4.2). This is illustrated again by the smaller (17 m wide) sinkhole type feature F2 present at the center of ST (Figures 3.2 and 3.5). Features F1 and F2 are inferrred to be small-scale (by the terms of this study) buried depression features having approximately 5 m of vertical relief.

In addition, it is possible that the large extent of the troughs may be the sole driving force for drainage. Nevertheless, the smaller features should not be ignored. Both the large troughs and smaller features play a role in the surface and subsurface drainage patterns (Figure 4.4), though, to what degree is not known and is beyond the scope of this study. Another joint possibility may be that NT and ST may have originated as smaller features such as F1 and F2 and by further development are the troughs seen today. If this possibility were true, then the next plausible thought would be that the troughs may still be developing, growing in length, width and depth. This is a geologic hazard that needs further attention. Gradual karst development with pre-exisiting drainage voids and the growing development in this area may very likely lead to a catastrophic event. Verification of this thought or proof of concept could be an interesting future study for this study site.

5. Summary and Conclusions

A premise of this study is that topographic indicators may precede sinkhole collapse events. To test this, identified surficial indicator features are compared with structures mapped with a conventional method for profiling the subsurface, ground penetrating radar (GPR). This study utilizes surfaces derived from airborne LIDAR (LIght Detection and Ranging) technology and compares them to subsurface horizons, in the attempt to observe the relationship between surficial and subsurface features within a karst terrain. The results suggest that airborne LIDAR may be used to map subtle topographic features associated with sinkhole hazard.

More than 500 km of LIDAR data were collected over central Florida by NASA's Airborne Topographic Mapper (ATM) in 1995. This data was processed and filtered to produce digital elevation models of the 'bare-ground' surface having 2.5m horizontal resolution and a vertical accuracy of ~20 cm. Ground truth comparisons were accomplished using an electronic total station (ETS) to survey control points. The profiles extracted from the LIDAR data and the ETS profiles were all consistent and all had approximately 15 – 20 cm difference. This result demonstrates the accuracy of the ATM data used for this study and is within the reported error of the instrument given by Krabill and Martin, (1987) and Krabill et al. (1995b).

To identify closed, circular features that are possibly pre-collapse signatures, interactive computer visualization of color-shaded relief maps were completed. This revealed four features non-existent on USGS topographic maps as promising depressions at a 200 m by 600 m site located in Apopka, Florida. This area was then selected as the focus study site for a more detailed investigation. In order to determine the minimum

size feature resolvable, the LIDAR DEM of the study site was compared with a similar resampled DEM derived from a USGS topographic map of the area. The difference between them was found to be approximately 2 m. The main result is that the USGS DEM did not depict the true ground surface as well as the LIDAR derived DEM. The bottom of basins seemed to be interpreted within the tree canopy and this is due in part to the technique used in preparing the USGS topographic maps.

The subtle topographic targets were verified by a GPR survey in the summer of 1999. The transects were guided by the ETS surveyed flag stations and their locations were chosen to obtain the best possible cross-section of the identified study site targets. Eight profiles were collected by towing the GPR antenna behind a vehicle across the ground. The main features resolved were two horizon surfaces, H1 and H2. They represent the top and bottom boundaries of a clay-rich layer approximately 10 m below. Within these interpreted horizons there are three large scale features; two troughs,one in the north portion of the site and the other in south (NT and ST) and a topographic high area (TH) towards the center of the site. A closer examination of the troughs in the GPR profiles found five smaller scale features (F1 – F5). Only two of the small-scale features correlated with the larger troughs NT and ST, they are F1 and F2, respectively. The other three were discarded for lack of supporting data. The features are inferred to be buried karst structures associated with sinkhole development.

To be able to visualize and compare the data, the GPR profiles were digitized into a GIS. Several maps were constructed, the most useful being 3-D continuous surfaces of the topography and the subsurface horizons. Initially, the TIN method was used. Unfortunately this produced unrealistic surfaces due to sharp angular artifacts that may

have beeen misinterpreted. To correct for this, the TINs were interpolated onto a regularly spaced, 1 m size raster grid and a low pass filter was applied. The filter used was an 11 m rectangular moving focal mean filter chosen for its ability to smooth the gridded surfaces into a representation more suitable of the true study site topography

The LIDAR derived surface correlated well with the three major subsurface structures in the GPR data (NT, ST and TH). Of the several smaller scale features identified in the clay rich layer, two have been used in this study. Features F1 and F2 correlate well with the surface topography and with the larger trough features (NT and ST, respectively). These have good GPR control and are thought to be small paleo-sinkholes or subsidence associated with the NT and ST. F1 and F2 may also be interpreted as sediments raveling downward with groundwater flow into unseen cavities in the limestone below. They may also be diffracted images from the trough edges.

Since, the ground penetrating radar did not reach the depth of limestone it is impossible to directly associate surface topography with subsurface voids. However, depressions and features in the overlying sediments are indirect evidence of buried solution cavities. Chen and Beck (1989) describe a model of the cover-collapse sinkhole process, where the gravitational movement of overburden sediment down into voids is a major factor in sinkhole development. In their model, very small openings in the limestone surface created sinkholes tens of times larger, if sufficient void space was available. Though, futher case studies are needed, the study site topography may reflect occurrences and developments in the subsurface.

This study indicates that to some degree, future sinkholes may be predicted by topographic indicators on a large scale. For example, in developing large areas for

schools, government buildings, office and shopping centers or large neighborhoods, LIDAR can be employed quickly, and is time and cost-effective. With the present technology available, initial visualization can be done almost immediately after the data is collected. This analysis would determine if there are any anomalies on the surface that the developer should be aware of. This information can then be taken to an environmental or geo-technical investigative firm to have the identified target features existence determined further. This can be accomplished using GPR as in this study or some other subsurface investigation method such as, electric resistivity, induced polarization, electromagnetic (EM) induction, hand or mechanical coring. Depending on the size of the area to be developed, this can be done in a matter of weeks. In contrast, by using only conventional subsurface methods, large amounts of time and money is wasted on evaluating too much area, in hopes that if suspicious features do exist, they will show up in the field data collected. For large areas, this take a lot of man power which is expensive and also time consuming.

Sinkholes are geologic hazards that due to their inherent suddenness become exceedingly dangerous. Ultimately sinkholes are connected to the surface, therefore high-resolution detailed topography mapping is useful as an aid or alternative to mapping the subsurface. By comparing conventional GPR derived surfaces to airborne LIDAR derived surfaces, this study has shown that inferences can be made about the surface from the LIDAR data. It is also shown that employing LIDAR technology for topographic mapping would yield topographic maps of higher resolution, accuracy and confidence in the contour values. These applications demonstrate that Airborne LIDAR is a useful tool for solving societal problems.

REFERENCES

Bates, R. L. and J. A. Jackson (1984). Dictionary of Geological Terms. New York, Double Day.

Beck, B. F. (1986). A generalized genetic framework for the development of sinkholes and karst in Florida, USA. Environmental Geologic Water Science 8 (12) pp. 5-18.

Beck, B. F. and S. Sayed (1991). The sinkhole hazard in Pinellas County: A geologic summary for planning purposes. Winter Park, FL, Florida Sinkhole Research Institute.

Benson, R.C. and L. Yuhr (1993). Spatial Sampling Considerations and their Applications to Characterizing Fractured Rock and Karst systems. Applied Karst Geology, Beck (ed.) pp.99-113.

Boyle Engineering Corporation (1997). Consumptive use Permit Application No. 2-095-0097 ANGM4R City of Apopka, Orange County – Results of Well Construction and Aquifer Performance Testing, 21 p.

Chen J. and B.F. Beck (1989). Qualitative Modelling of the Cover-collapse Process. Proceedings of the Third Multidisciplinary Conference on Sinkholes: St. Petersburg, Florida. A.A Balkema Publishers pp.89-95.

Church, R. H. and W. E. Webb (1985). Evaluation of a Ground penetrating radar system for detecting subsurface anomalies, Bureau of mines, U.S. Department of the Interior.

Cooper, S.S. and R.F. Ballard (1988). Geophysical Exploration for Cavity Detection in Karst Terrain. Geotechnical Aspects of Karst terrains Special Volume. New York, NY, American Society of Civil Engineers pp. 25-39.

Culshaw, M. G. and A. C. Waltham (1987). Natural and Artificial cavities as ground engineering hazards. Journal of Engineering Geology 20 pp.139 - 150.

Davis, J.L. and A.P. Annan, (1989). Ground-Penetrating Radar for High-Resolution Mapping of Soil and Rock Stratigraphy. Geophysical Prospecting 37 no. 5 pp.531–551.

Florida Geological Survey (FGS), (1986). Hydrogeologic Units of Florida, Florida Geological Survey Special Publication No. 28, Tallahassee, Florida, 9 p.

Federal Geographic Data Committee (FGDC), (1998). Geospatial Positioning Accuracy Standards, Part 3: National Standard for Spatial Data Accuracy, FGDC-STD-007.3-1998, 25 p.

Fetter, C.W. (1994). Applied Hydrogeology. Upper Saddle River, NJ, Prentice Hall., 691 p.

Ford, D. C. and P. W. Williams (1989). Karst Geomorphology and Hydrology, Unwin Hyman Ltd.

Guenther, G.C., Brooks, M.W., and LaRocque, P.E. (2000). New Capabilities of the "SHOALS" Airborne Lidar Bathymeter. Remote Sensing of Environment, 73 pp.247-255.

Hinds, N. E. A. (1943). Geomorphology: The Evolution of Landscape. New York, Prentice - Hall, Inc.

Jammal and Associates, Inc. (1982). The Winter Park Sinkhole, Geotechnical Engineering Report, submitted to the city of Winter Park, Florida by Jammal and Associates, Inc., Winter Park, Florida, 274 p.

Krabill, W.B. and J.G. Collins, (1984). Airborne laser topographic mapping results. Photogrammetry Engineering and Remote Sensing, 50 pp.685 - 694.

Krabill, W.B. and C. F. Martin, (1987). Aircraft Positioning using Global Positioning System carrier phase data. Navigation, 34 pp.1 - 21.

Krabill, W.B., R.H. Thomas, K. Jezek, K. Kuivinen and S. Manizade, (1995a). Greenland Ice Sheet Thickness Changes measured by Laser Altimetry. Geophysical Research Letters, 22 no. 17 pp.2341-2344.

Krabill, W.B., R.H. Thomas, C.F. Martin, R.N. Swift, and E.B. Frederick, (1995b). Accuracy of Airborne Laser Altimetry over the Greenland Ice sheet. International Journal of Remote Sensing 16 pp.1211 - 1222.

Krabill, W.B., C.W. Wright, R.N. Swift, E.B. Frederick, S.S. Manizade, J.K. Yungel, C.F. Martin, J.G. Sonntag, M. Duffy, W. Hulslander and J.C. Brock, (2000). Airborne Laser Mapping of Assateague National Seashore Beach. Photogrammetric Engineering & Remote Sensing 66 no.1 pp. 65-71.

McMechan, G.A., R.G. Loucks, X. Zeng, and P. Mescher (1998). Ground penetrating radar imaging of a collapsed paleocave system in the Ellenburger dolomite, central Texas. Journal of Applied Geophysics 39 pp.1-10.

Mellet, J.S. (1990). Ground-penetrating radar enhances knowledge of earth's surface layer. Geotimes pp.12-14.

Miller, J. A. (1986). Hydrogeologic Framework of the Floridan Aquifer system in Florida and parts of Georgia, Alabama and South Carolina. U.S. Geological Survey Professional Paper no. 1403-B. 91p.

Miller, J., (1997). Hydrogeology of Florida, The Geology of Florida. A. Randazzo and D. Jones eds., Gainesville, Florida, University Press of Florida pp. 69-88.

Newton, J.G., (1984). Review of Induced Sinkhole Development, Sinkholes: Their Geology, Engineering and Environmental Impact, B. Beck ed., A.A. Balkema Pub., Rotterdam, pp. 3-10.

Philpotts, A.R., N.H. Gray, M. Carroll, R.P. Steinen and J.B. Reid, (1997). The Electronic Total Station - A versatile, revolutionary new geologic mapping tool. Journal of Geoscience Education 45 pp. 38-45.

Randazzo, A. F. (1997). The Sedimentary Platform of Florida: Mesozoic to Cenozoic, The Geology of Florida. A. Randazzo and D. Jones eds., Gainesville, Florida, University Press of Florida pp. 39 - 56.

Ritchie, J.C., (1995). Airborne Laser Altimeter Measurements of Landscape Topography, Remote Sensing of the Environment 53 pp. 91-96.

Ritchie, J.C., (1996). Remote sensing applications to hydrology: airborne laser altimeters, Hydrological Sciences 41 no.4.

Ritchie, J.C., M. Menenti, and M.A. Weltz, (1996). Measurements of Land Surface Features Using an Airborne Laser Altimeter: the HAPEX-Sahel experiment. International Journal for Remote Sensing 17 no.18 pp.3705-3724.

Schmidt, W. (1997). Geomorphology and Physiography of Florida, The Geology of Florida. A. Randazzo and D. Jones eds., Gainesville, Florida, University Press of Florida pp. 1 - 12.

Scott, T. M. and M. Hajishafie (1980). Top of Floridan Aquifer in the St. Johns River Water Management District, Florida Bureau of Geology.

Scott, T.M. (1997). Miocene to Holocene History of Florida, The Geology of Florida. A. Randazzo and D. Jones eds., Gainesville, Florida, University Press of Florida pp. 57-68.

Sinclair, W. C. (1982). Sinkhole Development from Groundwater Withdrawal in the Tampa area, Florida. Tampa, Fl, U.S. Geolgical Survey, 19 p.

Sinclair, W.C. and J.W. Stewart, (1985). Sinkhole Type, Development, and Distribution in Florida, Florida Geological Survey Map Series No. 110, Tallahassee, Florida, 1 p.

Sinclair, W.C., J.W. Stewart, R.L. Knutilla, A.E. Gilboy, and R.L. Miller, (1985). Types, Features and Occurence of Sinkholes in the Karst of West-Central Florida, U.S. Geological Survey Water Resources Investigations Report No. 85-4126, Tallahassee, Florida, 81 p.

Spencer, S.M. and E. Lane, (1995). Florida Sinkhole Index, Florida Geological Survey Open File Report No. 58, Tallahassee, Florida, 18 p.

Stangland, H.G. and S.S. Kuo (1987). Use of Ground Penetrating Radar Techniques to Aid in Site Selection for Land Application Sites. Karst Hydrogeology. Proceedings 2nd Conference, Orlando, Florida. pp.171-177.

Topp, G.C., J.L. Davis and A.P. Annan (1980). Electromagnetic Determination of Soil and Water Content: Measurements in coaxial transmission lines. Water Resources Research 16 no.3 pp.574-582.

United States Geological Survey (USGS), (1993). Digital Elevation Models -data users guide 5, Reston, Virginia, U.S. Geological Survey, 48 p.

Upchurch, S. and A. Randazzo (1997). Environmental Geology of Florida, The Geology of Florida. A. Randazzo and D. Jones eds. Gainesville, Florida, University Press of Florida, pp. 217-250.

Vaughn, C.R., J.L. Bufton, W.B. Krabill and D. Rabine, (1996). Georeferencing of Airborne Laser Altimeter Measurements. International Journal of Remote Sensing, 17 no.11 pp. 2185 - 2200.

White, W.A. (1970). The Geomorphology of the Florida Peninsula, Florida Bureau of Geology Bulletin No. 51, Tallahassee, Florida, 164 p.

Whitman, D., T. Gubbels, and L. Powell (1999). Spatial Interrelationships between Lake Elevations, Water Tables, and Sinkhole Occurrence in Central Florida: A GIS Approach. Photogrammetric Engineering & Remote Sensing 65 pp. 1169-1179.

Whitman, D., (2000). 1999-2000 ALTM Data Collected in Eastern Broward County, Florida, Broward County Commission Emergency Management Division, Plantation, Florida, 27 p.

Whitman, D., K. Zhang, S. Leatherman and W. Robertson, (2001). Airborne Laser Topographic Mapping: Applications to Hurricane Storm Surge Hazards. AGU "Earth Science in the Cities" Series in press.

Wilson, W. L. and B. F. Beck (1988). Evaluating Sinkhole Hazards in Mantled Karst Terrain. Geotechnical Aspects of Karst Terrains Special Volume. New York, NY, American Society of Civil Engineers, pp. 1-25.

Wilson, W. L. and B. F. Beck (1992). Hydrogeologic Factors Affecting New Sinkhole Development in the Orlando Area, Florida. Ground Water 30 pp. 918 – 930.

Wilson, W.L. (1998). Basic Principles of Ground Penetrating Radar, Subsurface Evaluations, Inc., Tampa, Florida, 27 p.

APPENDIX

GLOSSARY OF ACRONYMS

ATM: NASA's Airborne Topographic Mapper instrument

DEM: Digital Elevation Model

GIS: Geographic Information Systems

GPR: Ground Penetrating Radar

GPS: Global Positioning System

INS: Inertial Navigation System

LIDAR: LIght Detection and Ranging

NAD27: North American Datum of 1927

NAD83: North American Datum of 1983

NAVD88: North American Vertical Datum of 1988

NGS: National Geodetic Survey

NGVD29: National Geodetic Vertical Datum of 1929

RMSE: Root-Mean-Square-Error

UTM: Universal Transverse Mercator

RADAR: Radio detecting and Ranging

SFWMD: South Florida Water Management District

SJRWMD: St. Johns River Water Management District

SWFWMD: South West Florida Water Management District

TWTT: Two-Way Travel Time

USGS: United States Geological Survey